(12)

N60921-81-C-0229

INVESTIGATION OF LITHIUM THIONYL CHLORIDE BATTERY SAFETY HAZARDS

GTE COMMUNICATIONS PRODUCTS CORPORATION
STRATEGIC SYSTEMS DIVISION
POWER SYSTEMS OPERATION
520 WINTER STREET
WALTHAM, MASSACHUSETTS 02154

JANUARY 1983

TECHNICAL REPORT N60921-81-C-0229
FINAL REPORT FOR PERIOD SEPT 1981 TO NOV 1982

Approved for public release; distribution unlimited.

NAVAL SURFACE WEAPONS CENTER
WHITE OAK, SILVER SPRING, MD 20910
CODE R33

GTE Systems

Strategic Systems Division
GTE Communications Products Corporation

N60921-81-C-0229

INVESTIGATION OF LITHIUM THIONYL CHLORIDE BATTERY SAFETY HAZARDS

GTE COMMUNICATIONS PRODUCTS CORPORATION
STRATEGIC SYSTEMS DIVISION
POWER SYSTEMS OPERATION
520 WINTER STREET
WALTHAM, MASSACHUSETTS 02154

JANUARY 1983

TECHNICAL REPORT N60921-81-C-0229
FINAL REPORT FOR PERIOD SEPT 1981 TO NOV 1982

NAVAL SURFACE WEAPONS CENTER
WHITE OAK, SILVER SPRING, MD 20910
CODE R33

GTE Systems

Strategic Systems Division
GTE Communications Products
Corporation

BLANK PAGES
IN THIS
DOCUMENT
WERE NOT
FILMED

SECURITY CLASSIFICATION OF THIS PAGE (When Data Entered)

REPORT DOCUMENTATION PAGE

READ INSTRUCTIONS BEFORE COMPLETING FORM

1. REPORT NUMBER: N60921-81-R-0190	2. GOVT ACCESSION NO.: A129302
3. RECIPIENT'S CATALOG NUMBER:	
4. TITLE (and Subtitle): Investigation of Lithium Thionyl Chloride Battery Safety Hazard	5. TYPE OF REPORT & PERIOD COVERED: Final Sept. 1981-Nov. 1982
	6. PERFORMING ORG. REPORT NUMBER:
7. AUTHOR(s): Robert C. McDonald, Frederick W. Dampier Co-investigators: Paul Wang, James M. Bennett	8. CONTRACT OR GRANT NUMBER(s):
9. PERFORMING ORGANIZATION NAME AND ADDRESS: GTE Communication Products Corp. Strategic Systems Division/Power Systems Op. 520 Winter St., Waltham, MA 02154	10. PROGRAM ELEMENT, PROJECT, TASK AREA & WORK UNIT NUMBERS:
11. CONTROLLING OFFICE NAME AND ADDRESS: Naval Surface Weapons Center White Oak, Silver Spring, MD 20910 Code R33	12. REPORT DATE: January, 1983
	13. NUMBER OF PAGES:
14. MONITORING AGENCY NAME & ADDRESS(if different from Controlling Office):	15. SECURITY CLASS. (of this report):
	15a. DECLASSIFICATION/DOWNGRADING SCHEDULE:

16. DISTRIBUTION STATEMENT (of this Report)

Approved for Public Release; Distribution Unlimited

17. DISTRIBUTION STATEMENT (of the abstract entered in Block 20, if different from Report)

18. SUPPLEMENTARY NOTES

19. KEY WORDS (Continue on reverse side if necessary and identify by block number)

Lithium, Thionyl Chloride, Battery, Safety, Overdischarge, Discharge, Intermediates, Raman, Infrared, Electron Spin Resonance, Dendrites

20. ABSTRACT (Continue on reverse side if necessary and identify by block number)

The chemistry of discharge and overdischarge in Li/$SOCl_2$ cells has been examined with Raman emission, Fourier transform infrared, and electron spin resonance spectroscopies to determine if any hazardous reactions can occur. Under moderate discharge rate at room temperature, the electrolyte from discharged and cathode limited overdischarged cells contains primarily $LiAlCl_4$.3 SO_2, $LiAlCl_4$.2 $SOCl_2$, and perhaps $LiAlCl_4.SOCl_2.SO_2$; traces of $SO_3^=$ are indicated. Three free radicals

DD FORM 1 JAN 73 1473 EDITION OF 1 NOV 65 IS OBSOLETE

SECURITY CLASSIFICATION OF THIS PAGE (When Data Entered)

are present at low concentrations on discharge and cathode limited overdischarge with two additional radicals appearing on extended anode limited overdischarge. At least one of these is cationic polymeric sulfur. Both FTIR and ESR suggest intermediates exist with lifetimes on the order of days from discharge and overdischarge. No hazardous reactions were observed at anytime. Pressure from SO_2, a principal result of discharge, remains low due to the $LiAlCl_4.3SO_2$ complex in solution. Scanning electron and optical microscopic investigations of overdischarged cathodes reveal a three-dimensional reticulated lithium dendrite structure. Individual dendrites do not grow any longer than about 50 microns or any thicker than about four microns in diameter before branching at random angles. The extent of dendritic growth and the fate of the dendrites depends on the discharge conditions. No overdischarged hazards were encountered in this study though several hazard scenarios suggested themselves.

FOREWORD

This report describes the effort conducted under Contract N60921-81-R-0190 awarded by Naval Surface Weapons Center, White Oak, Silver Spring, MD 20910. It was funded by the High Energy Batteries for Weapons Block Program (SF65-571-692), with Dr. William P. Kilroy as Technical Monitor. This is the final report on the work performed during the period of September 1981 through November 1982.

The work reported herein was performed under the direction of Dr. Robert C. McDonald. The report was released by the author in December 1982.

The author wishes to thank Mr. James M. Bennett, Dr. Frederick W. Dampier, and Mr. Paul Wang for their contributions as co-investigators on this project.

TABLE OF CONTENTS

LIST OF ILLUSTRATIONS

LIST OF ILLUSTRATIONS (Cont)

LIST OF TABLES

1.0 INTRODUCTION

Reports of cell ruptures and explosions on overdischarge of lithium/thionyl chloride and lithium/sulfur dioxide batteries/cells have circulated for a number of years. Among the studies resulting from these events was one carried out by Abraham et al[1, 2] in which it was proposed that Li_2S is found in cathode limited cells, and SCl_2, Cl_2 and a material with infrared absorption at $1070cm^{-1}$ are formed in anode limited cells. The principal techniques employed were cyclic voltammetric and infrared spectroscopy. Although explosions were found to occur in anode limited wound C cells on overdischarge, no specific chemical species or reaction mechanism was implicated.

A second study reported by Salmon et al[3] revealed the presence of a species, perhaps Cl_2O, which forms in $Li/SOCl_2$ cells following removal of a relatively high applied overdischarge current from a cathode limited cell. It was speculated, still without a detailed mechanism, that decomposition of Cl_2O accounts for occasional explosions on cell reversal.

GTE Sylvania has performed a considerable number of overdischarge tests on D cells and 10,000 Ah Minuteman cells[4, 5, 6, 7, 8] in actual application series modes without observing cell hazards. However, these were 1 mA/cm^2 discharge applications in anode limited cells. During such a controlled low rate overdischarge in anode limited cells, it is believed that the forced oxidation products (e.g. SO_2Cl_2, Cl_2) recombine rapidly with the forced reduction products (e.g. lithium metal dendrites) so that no sudden exothermic reaction takes place during or following overdischarge. However, this hypothesis must be verified experimentally. Furthermore, it has been known for some years that, as emphasized by Kilroy and James[9], intimate mixture of lithium, carbon, and thionyl chloride are extremely unstable. The implication is that in circumstances such as high rate overdischarge which may generate carbon/lithium matrices, a carbon catalyzed explosive reaction may occur between lithium and $SOCl_2$ or other reactive species.

GTE has established a basis for understanding the $Li/SOCl_2$ discharge mechanism (Schlaikjer)[10] and has performed preliminary studies on the infrared and Raman spectra of discharge products. The characterization of overdischarge products and secondary reactions is a logical extension of this work.

The second focus of this work was the examination in situ of lithium deposition and dendrite formation in lithium/thionyl chloride cells during both cathode and anode

limited overdischarge, recording the observations photographically. Optical microphotographs were taken of the dendrites while they were immersed in the $SOCl_2$ electrolyte during overdischarge or storage and later the dendrite morphology was examined at magnifications up to 3000X by scanning electron microscopy (SEM). Carbon from the cathodes was analyzed by X-ray diffraction to identify the discharge products. The objective of the study was to determine whether deposited lithium and other products of overdischarge could cause hazardous spontaneous thermal excursions or explosions.

2.0 RAMAN EMISSION SPECTROSCOPY

2.1 EXPERIMENTAL

Details of the Raman experimental setup are given in QR-1*. All Raman spectra reported were from electrolyte, removed from cells, and sealed in quartz tubes with a MAAP gas torch. An effort was made to collect spectra in situ with a sealed glass cell. The electrolyte volume was apparently too large (approximately 70 times the normal cc/Ah ratio) and no emission, in addition to those of fresh electrolyte, were detected through anode limited overdischarge.

2.2 RESULTS

Control spectra were provided in QR-1 for sulfur and SO_2 in electrolyte. No significant difference can be seen between Raman spectra of discharged electrolyte and cathode limited overdischarged electrolyte. Spectra for discharged and overdischarged electrolyte are shown in Tables 1, 2, and 3. Assignments are made by comparison with controls and literature values.

2.3 DISCUSSION

Recently, Barbier et al[11] have presented data from Raman spectroscopy, phase studies, and X-ray crystallography to support the existence at room temperature of the additional compounds: $LiAlCl_4 \cdot 3\ SO_2$, $LiAlCl_4 \cdot 2\ SOCl_2$, and $LiAlCl_4 \cdot SOCl_2 \cdot SO_2$. Nearly all of the Raman peaks for discharged electrolyte can be accounted for with these results. These strong complexes formed in solution explain the low partial pressures observed for SO_2 and $SOCl_2$ in discharged practical cells[12].

If indeed most of the oxides and oxychlorides of sulfur do form adducts in $SOCl_2$ with $LiAlCl_4$ or $AlCl_3$, then some caution must be exercised in comparing spectroscopic literature data derived from other solvent systems, gas phase, or solid argon matrix experiments, since the Lewis acid will radically change the electronic and atomic structure.

QR-N signifies the nth quarterly report.

TABLE 1
RAMAN SPECTRUM OF 100% DISCHARGED ELECTROLYTE

νObserved	νAssigned	Assignment	Reference
209 M	204	$LiAlCl_4$ 2 $SOCl_2$	QR-I,(11)
280 VW, Sh	284	$SOCl_2$	(13)
304 W	299	$LiAlCl_4$ 2 $SOCl_2$	
333 VW	345	$SOCl_2$	(13)
354 S, Asym	359	$LiAlCl_4$ 2 $SOCl_2$	(11)
473 W, Sh	478	Sulfur	QR-I
505 M	502	$LiAlCl_4$ 2 $SOCl_2$	QR-I,(11)
601 VW			
1162 W	1161	$LiAlCl_4$ 3 SO_2	(11)
1223 VW br	1223	$LiAlCl_4$ 2 $SOCl_2$	(11)
1336 VW br	1332	SO_2	(14)

TABLE 2
RAMAN SPECTRUM OF 30% CATHODE LIMITED OVERDISCHARGED ELECTROLYTE

νObserved	νAssigned	Assignment	Reference
210 M	204	$LiAlCl_4$ 2 $SOCl_2$	QR-I
280 W	284	$SOCl_2$	(13)
305 W		$LiAlCl_4$ 2 $SOCl_2$	
332 VW		$SOCl_2$	
358 M		$LiAlCl_4$ 2 $SOCl_2$	
475 M	478	Sulfur	QR-I
509 M	500	$LiAlCl_4$ 2 $SOCl_2$	QR-I
1159 W		$LiAlCl_4$ $3SO_2$	
1229VW		$LiAlCl_4$ $2SOCl_2$	

TABLE 3
RAMAN SPECTRUM OF 90% ANODE LIMITED OVERDISCHARGED ELECTROLYTE

νObserved	νAssigned	Assignment	Reference
96 S			
145 ASYM			
210 M	204	$LiAlCl_4 \cdot 2\ SOCl_2$	(11)
244 VW			
304 W	299	$LiAlCl_4 \cdot 2\ SOCl_2$	(11)
355 S	359	$LiAlCl_4 \cdot 2\ SOCl_2$	(11)
461 VW, Sh	465	$LiAlCl_4 \cdot 2\ SOCl_2$	(11)
480 VW, Sh	478	Sulfur	QR-I
491 VW, Sh	490	$SOCl_2$	(13)
510 M br	502	$LiAlCl_4 \cdot 2\ SOCl_2$	(11)
687 W			
727 W			
819 VW		$LiAlCl_4 \cdot 2\ SOCl_2$	By comparison with IR
854 VW			
1162 W	1157, 1161	$LiAlCl_4 \cdot 3\ SO_2$, $LiAlCl_4 \cdot 2\ SOCl_2$	(11)
1231 W			

We do not see a peak at 388 or 679 cm^{-1} in either IR or Raman discharged electrolyte spectra as suggested by Istone and Brodd for S_2O[15] which absorbs at 1165, 679, and 388 cm^{-1}. No evidence is seen for free molecular chlorine at 556 cm^{-1}[16], SO at 1125 cm^{-1}[14] or SOCl which would have its SO stretch near 1182 cm^{-1}. The very weak 601 cm^{-1} emission remains unaccounted for.

Therefore, the intermediates suggested for the $Li/SOCl_2$ cell by cyclic voltametry and ESR do not appear concentrated enough in discharged electrolyte to provide Raman emission.

The Raman spectrum from anode limited overdischarged electrolyte provides some new and unique emissions. They are difficult to identify at present but are probably due to oxide and oxychloride intermediates associated with solute complexes. There is no correlation between Raman emission and infrared absorption in the 600 - 1000 region except for a peak at 819 which has been ascribed to $SOCl_2$ and SO_2 complexes.

The Raman spectrum from cathode limited overdischarged electrolyte contains no emission different from that of discharged electrolyte.

3.0 INFRARED SPECTROSCOPY

3.1 EXPERIMENTAL

The details of instrumentation and sampling techniques were given in QR-I. In all cases, electrolyte was sampled from cells and examined on the spectrometer within four hours unless otherwise noted. All cells were discharged at room temperature at 1 mA/ cm^2.

As discussed in QR-III, controlled spectra taken of electrolyte stored in sealed glass and AgCl cells shows development in the latter of peaks at 767-783 cm^{-1}, 691 cm^{-1}, and 2450-3200 cm^{-1}. These four regions are therefore considered unreliable for the purposes of this study.

Improvements were made in obtaining better signal-to-noise ratio by tilting the cell in the laser beam and by the use of computer software for removal of interference fringes.

3.2 RESULTS

Infrared spectra are presented in Tables 4 and 5 along with tentative assignments and an indication of the peak change on storage.

No significant difference exists between spectra from discharged and cathode limited overdischarged electrolyte. Most of the infrared absorption can be accounted for by addition complexes with $LiAlCl_4$.

Peak positions change on standing for all discharge conditions, but the most striking changes take place in stored anode limited electrolyte.

3.3 DISCUSSION

Recent findings by Barbier et al[6] have shown the existence of $LiAlCl_4$ adducts with $SOCl_2$ and SO_2 analagous to $AlCl_3$ addition compounds. A complex of adduct equilibria thus exists for $SOCl_2$, SO_2 (Figures 1,2, and 3), and possibly the following other sulfur compounds:

$$LiAlCl_4 + 2\ SOCl_2 \rightleftharpoons LiAlCl_4 \cdot 2\ SOCl_2$$
$$LiAlCl_4 + 3\ SO_3 \rightleftharpoons LiAlCl_4 \cdot 3\ SO_2$$
$$LiAlCl_4 + SOCl_2 + SO_2 \rightleftharpoons LiAlCl_4 \cdot SOCl_2 \cdot SO_2$$
$$LiAlCl_4 \cdot 2\ SOCl_2 + SO_2 \rightleftharpoons LiAlCl_4 \cdot SOCl_2 \cdot SO_2 + SOCl_2$$

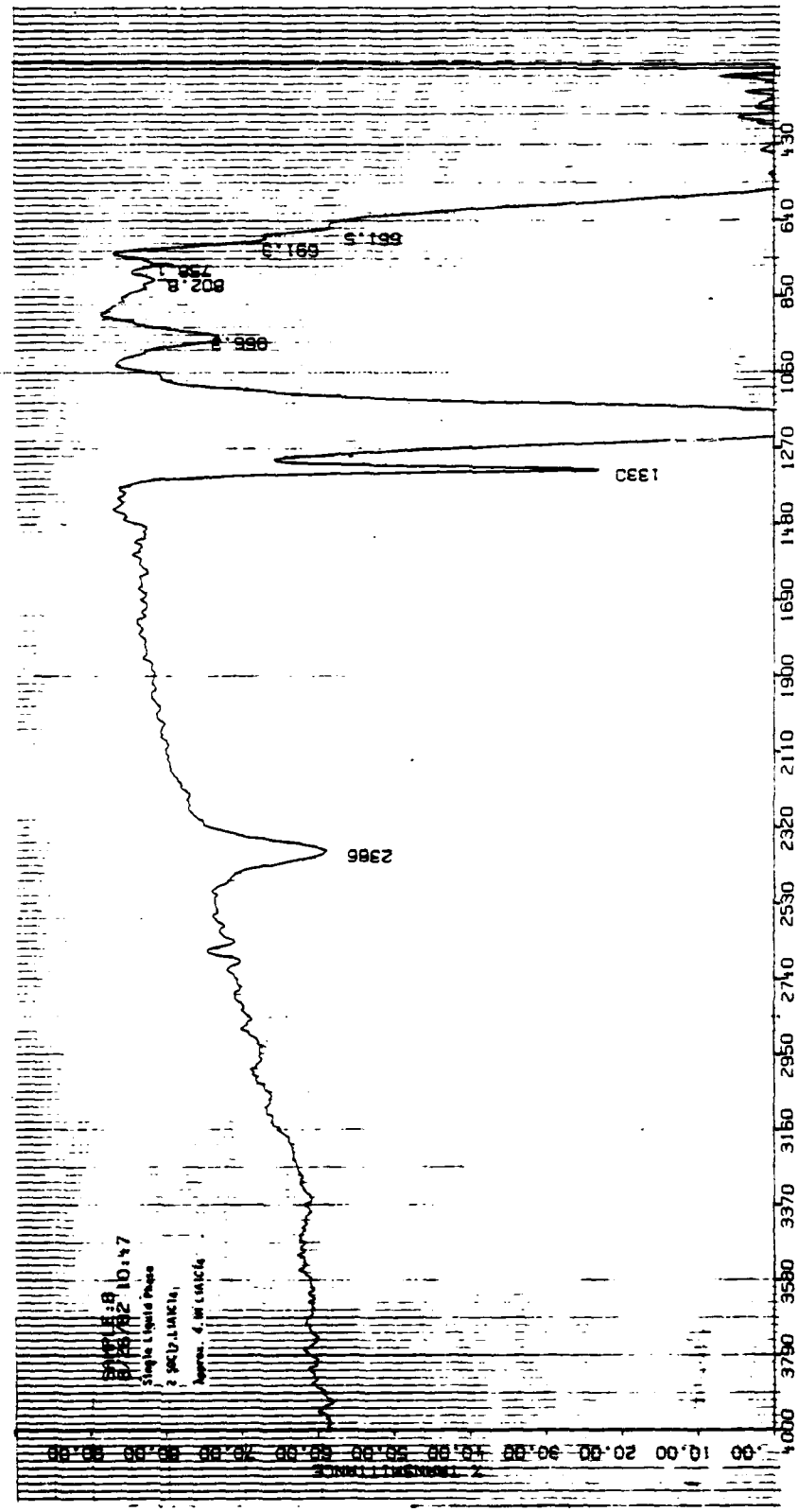

Figure 1. Infrared Spectrum of $LiAlCl_4$ 2 $SOCl_2$

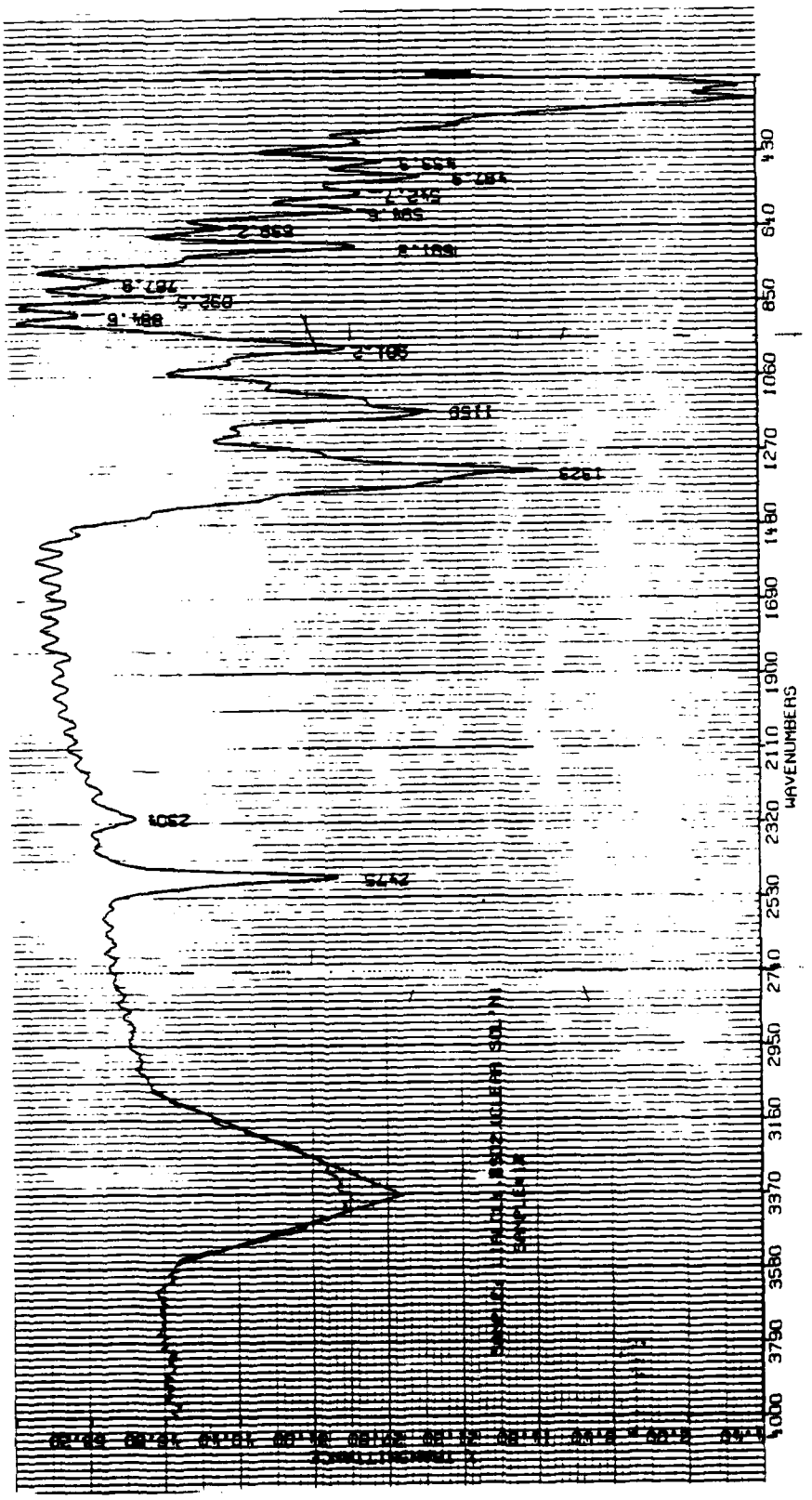

Figure 2. Infrared Spectrum of $LiAlCl_2 \cdot 3\ SO_2$

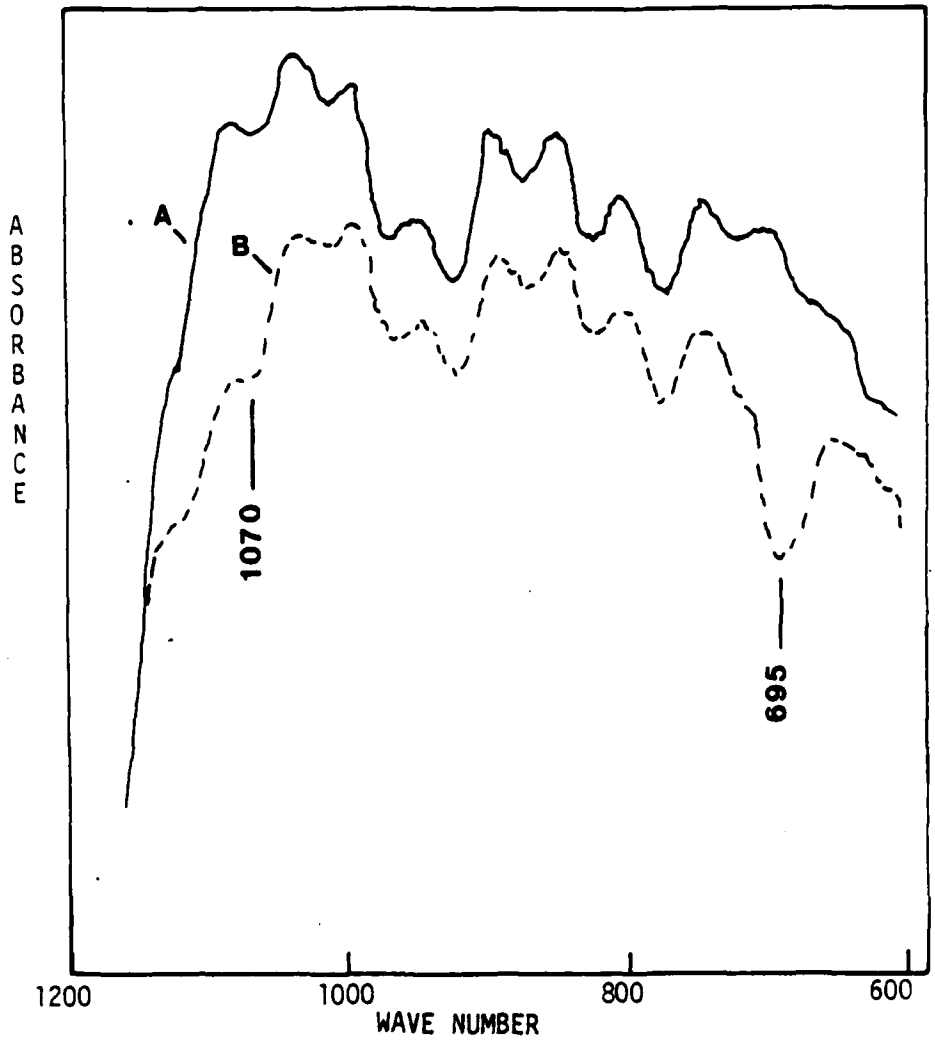

Figure 3. Refractive Infrared Spectra of (A) Electrolyte and (B) Electrolyte Containing SO_3

TABLE 4
INFRARED SPECTRUM OF DISCHARGED ELECTROLYTE

ν Observed	Change On Storage	ν Assigned	Assignment	Reference
654 - 661	-	661	$LiAlCl_4 \cdot SOCl_2$	Final
684	-			
702		699	$LiAlCl_4 \cdot 2\ SOCl_2$	Final
762	-	758	$LiAlCl_4 \cdot 2\ SOCl_2$	Final
		773	$SOCl_2$	QR-I (13)
802	-	802	$LiAlCl_4 \cdot 3\ SO_2$	Final
825	-	825	$LiAlCl_4 \cdot 2\ SOCl_2$	Final
966	Increase	966	$LiAlCl_4 \cdot 2\ SOCl_2$	Final
974	Decrease	981	$LiAlCl_4 \cdot 3\ SO_2$	Final
1070	Decrease	1070	SO_3	(17)
1330		1338	SO_2	QR-I
		1330	$LiAlCl_4 \cdot 3\ SO_2$	Final
2304	Increase	1152 + 1152	$LiAlCl_4 \cdot 3\ SO_2$	Final
2398 - 2401	Increase	1162 + 1223	$LiAlCl_4 \cdot 2\ SOCl_2$	Final
2468 - 2475	Increase	1323 + 1152	$LiAlCl_4 \cdot 3\ SO_2$	Final

TABLE 5
INFRARED SPECTRUM OF ANODE LIMITED OVERDISCHARGED ELECTROLYTE

ν Observed	Change On Storage	ν Assigned	Assignment	Reference
602				
661	Increase	661	$LiAlCl_4 \cdot 2\ SOCl_2$	Final
767				
773		773	$SOCl_2$	QR-I
787				
817-825		825	$LiAlCl_4 \cdot 2\ SOCl_2$	Final
802	Increase			
958	Decrease			
966	Increase	966	$LiAlCl_4 \cdot 2\ SOCl_2$	Final
1152	Decrease		SO_2	QR-I
1077 - 1085	Increase	1070	SO_3	(17)
1330-1338	Decrease	1337	SO_2	QR-I
1345-1354	Increase			
1397	Increase			
2297	Decrease	1152 + 1152	$LiAlCl_4 \cdot 3\ SO_2$	Final
2386-2393	Increase	1162 + 1223	$LiAlCl_4 \cdot 2\ SOCl_2$	Final
2468	Decrease			

Formation of the complexes is slow, so when SO_2 is formed in discharge, there may be some delay in forming the most stable complexes. With time, a stable trio of peaks near 2398 cm^{-1} develops which probably represents combinations of S-O stretching frequencies between 1100 and 1400 cm^{-1} for the more stable complexes. At this point, it would be difficult to assign frequencies for SO, $SOCl^{\cdot}$, and S_2O in the presence of $LiAlCl_4$. There is no evidence for SO_2Cl_2 (1414 cm^{-1}).

SO_3 is neither a Lewis acid nor base and might be expected to be unassociated in solution. Analysis by mass spectroscopy of the gas evolved in large 10,000 Ah cells reveals traces of SO_3[12]. The infrared peak at 1070 cm^{-1} (Figures 4 and 5) may result from a distorted SO_3 in solution. As suggested before[12], SO_3 may result from decay of active intermediates combining with trapped atmospheric air or other oxidizers.

$$SO + O_2 \rightarrow SO_3$$

$$2\,SOCl^{\cdot} + 2\,O_2 \rightarrow SO_3 + SOCl_2$$

$$2\,SO + SOCl_2 \rightarrow SO_3 + S_2Cl_2$$

$$2\,SOCl^{\cdot} + 2\,SO_2 \rightarrow 2\,SO_3 + S_2Cl_2$$

S_2Cl_2 is not easily identified by infrared but has been indicated by cyclic voltametry of discharged electrolyte[19, 20].

There is no significant difference between FTIR spectra for discharges and cathode limited overdischarges at $1mA/cm^2$ at room temperature. This is consistent with Raman and ESR data. The situation is evidently changed at much higher rates[3] but we have no data on this yet.

FTIR spectra of electrolyte from anode limited overdischarged cells (Figure 6) show some new detail at 1070, 662, and 966 cm^{-1} while SO_2 and $SOCl_2$ are still very much in evidence. Within days, however, the SO_2 complex absorbance at 1336 cm^{-1} disappears.

Peaks at 1070, 1345, and 802 grow in stored anode limited electrolyte. There is no evidence of SO(1136 cm^{-1}) or SO_2Cl_2 (1414 cm^{-1}) as reported in the literature. The peak at 691 cm^{-1} ascribed to Cl_2O[21] unfortunately overlaps a severe artifact.

Evidence for the presence of SO_3 in anode limited overdischarge comes from a number of sources. As shown in QRII, Li_2SO_4 saturated electrolyte (about 0.2M in sulfate equivalent) provides an infrared spectrum consistent with that for stored anode limited overdischarged electrolyte. It is believed that Li_2SO_4 dissociates according to

$$Li_2SO_4 \rightleftharpoons SO_3 + Li_2O$$

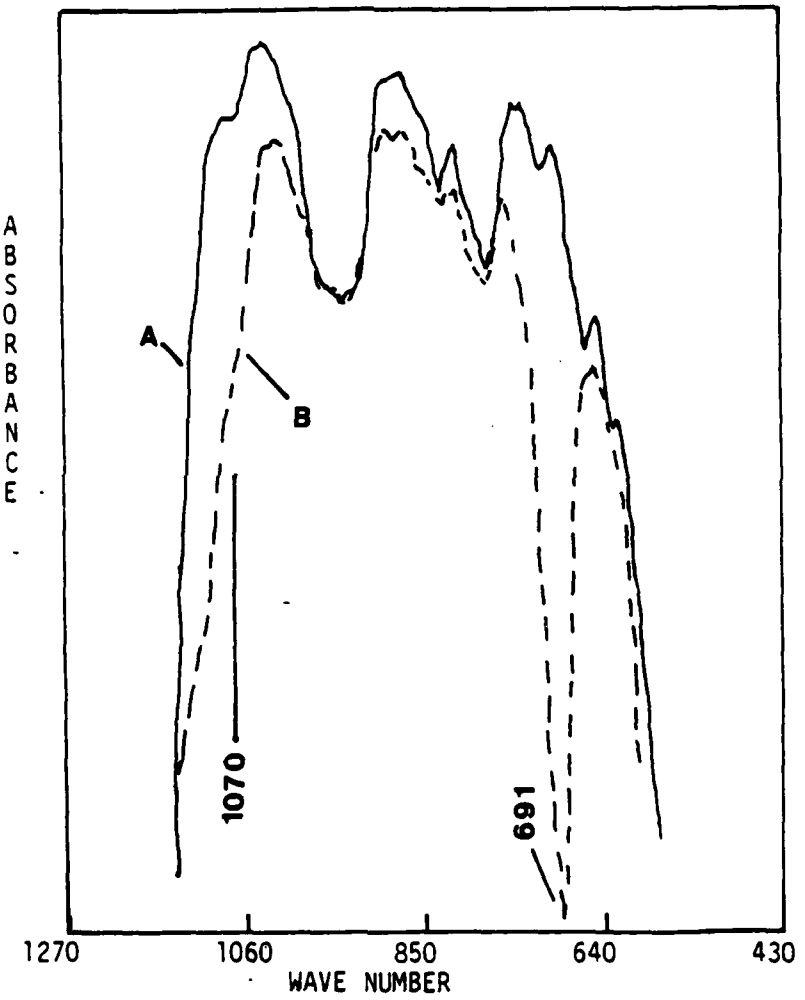

Figure 4. Infrared Spectra of (A) Electrolyte and (B) SO_3 Containing Electrolyte

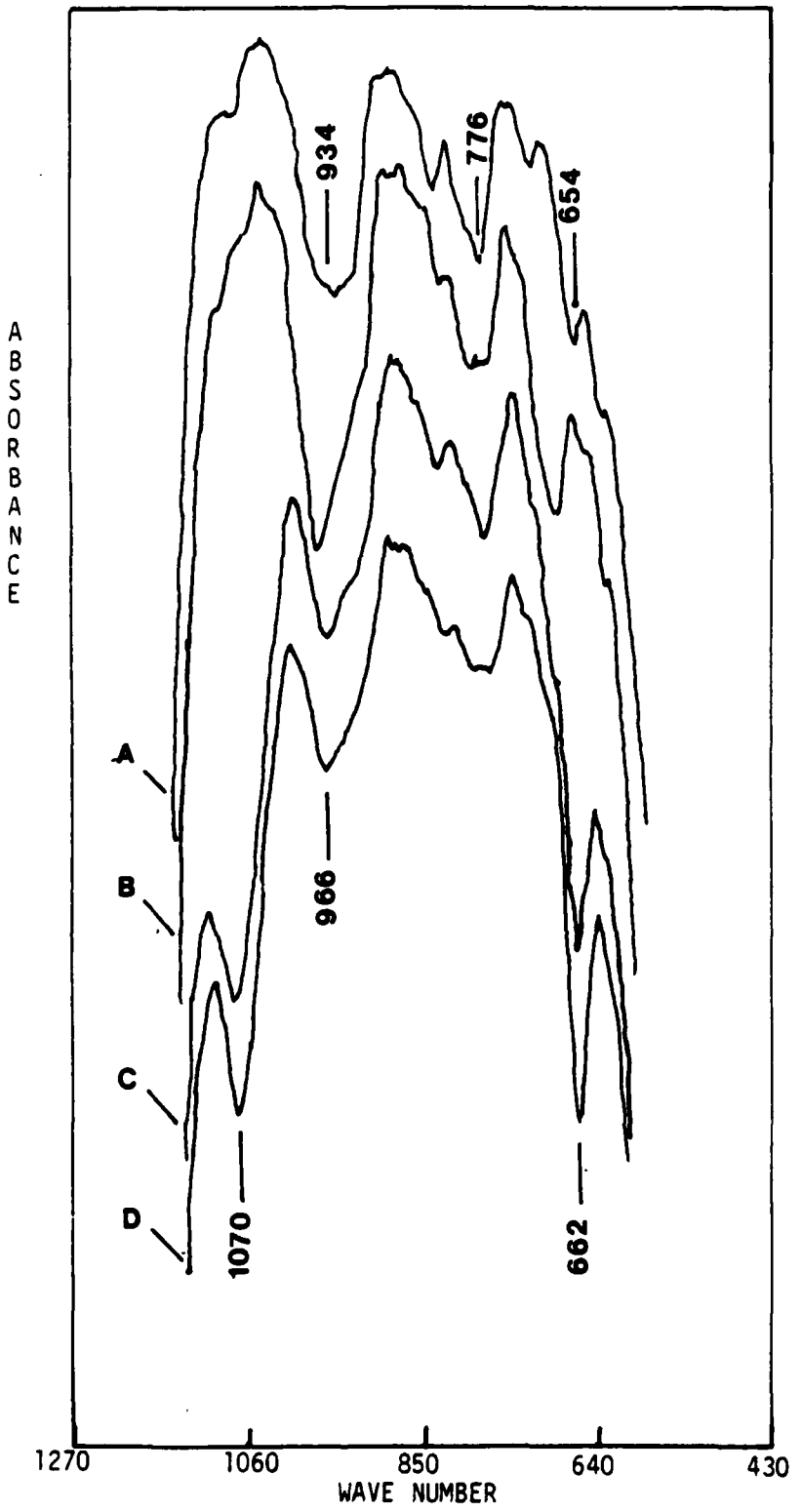

Figure 5. Infrared Spectra of (A) Fresh, (B) 97% Discharged, (C) 50% Anode Limited Overdischarged and (D) 100% Anode Limited Overdischarged Electrolyte

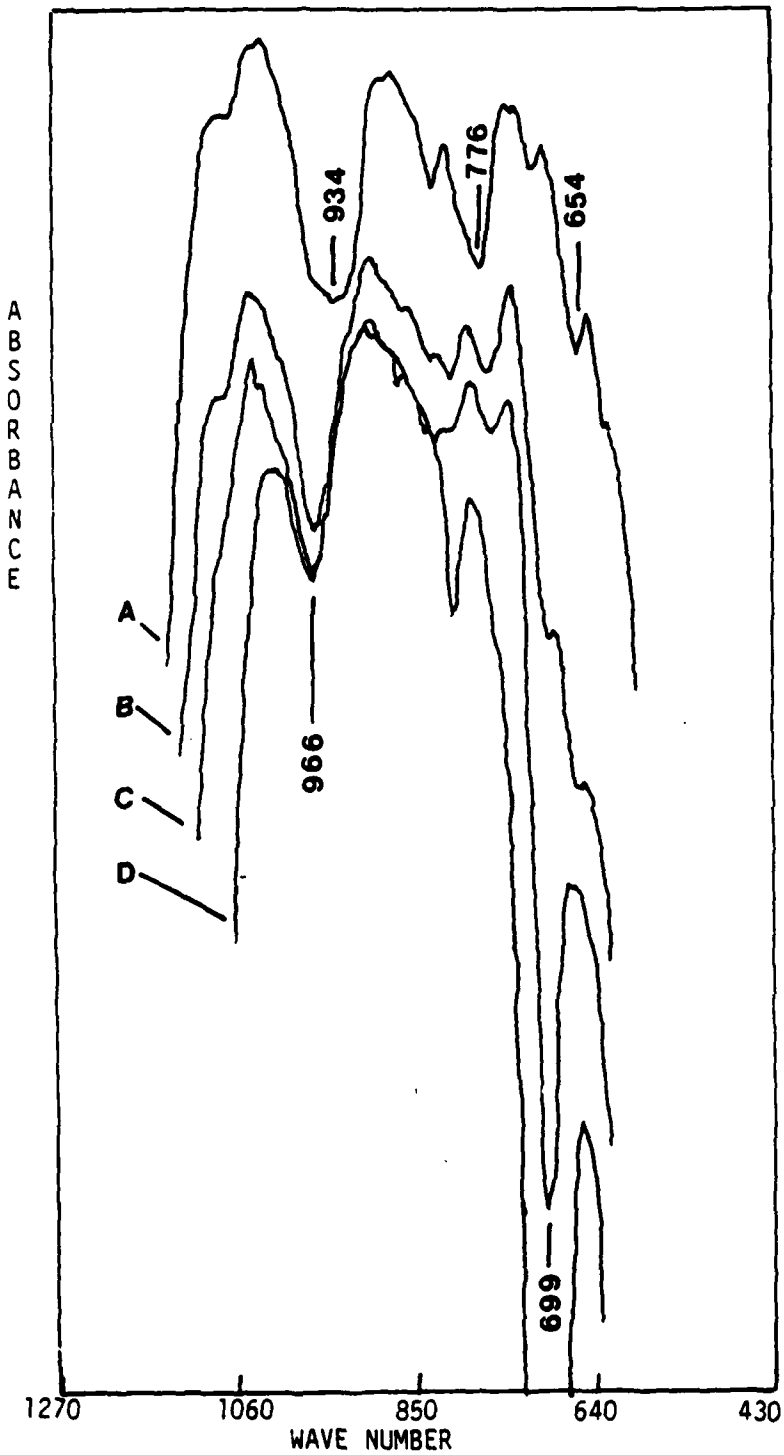

Figure 6. Infrared Spectra of (A) 10 m/o, (B) 30 m/o, (C) 50 m/o and (D) 60 m/o $LiAlCl_4$ in $SOCl_2$

since no free sulfate absorbances are found. Other results in this laboratory have suggested a similar equilibrium:

$$Li_2SO_3 \rightleftharpoons SO_2 + Li_2O$$

Figures 3 and 4 show the spectra of SO_3 solutions (not saturated) in electrolyte with no SO_2 present.

The SO_3 shows a characteristic absorbance at 1070 cm^{-1} in electrolyte though the Raman data[17] of pure planar SO_3 gas predicts that 1070 cm^{-1} is inactive in the infrared. Thus, SO_3 in electrolyte is not perfectly planar and most likely associated. The delay in formation of 1345 cm^{-1} and disappearance of 1336 cm^{-1} would be consistent with a rearrangement such as:

$$SO_3 + LiAlCl_4 \cdot SOCl_2 \cdot SO_2 \rightleftharpoons LiAlCl_4 \cdot SO_3 \cdot SO_2 + SOCl_2.$$

The marked stability and growth of 1070 cm^{-1} eliminates the highly unlikely SO^{+2} suggested by Salmon[21].

The details of SO_3 generation are still unclear. The approximate ease of oxidation of discharge products on discharge should be in opposite order to their potential vs lithium:

$$Li^{\circ} > AlCl_4^- >> S > SO_2 > SOCl_2 > SO_2Cl_2.$$

After lithium is consumed on overdischarge, the next most likely oxidations to occur would be:

$$AlCl_4^- \rightarrow AlCl_3 + 1/2\ Cl_2 + e^-$$

$$2\ S + 2\ AlCl_4^- \rightarrow S_2Cl_2 + 2\ AlCl_3 + 2e^-$$

$$S + 2\ AlCl_4^- \rightarrow SCl_2 + 2\ AlCl_3 + 2\ e^-$$

$$2\ SO_2 + 2\ AlCl_4^- \rightarrow SO_3 + SOCl_2 + 2\ AlCl_3 + 2\ e^-.$$

No chlorine is detected in the Raman. SCl_2 and S_2Cl_2 are not seen in either Raman or infrared nor have they been indicated from cyclic voltammetric studies in overdischarge. As we have seen though, there is evidence for SO_3. Regeneration of SO_2 and LiCl would occur as follows:

$$SO_3 + SOCl_2 + 2\ Li^{\circ} \rightleftharpoons 2\ SO_2 + 2\ \underline{LiCl}$$

since lithium dendrites are clearly abundant. Small amounts of SO_3 remain perhaps stabilized by complex formation or the exhaustion of available lithium on the cathode since there is more than one process which consumes the lithium.

A reasonable series of intermediate reactions to account for the additional free radicals observed on anode limited overdischarge is as follows:

$$SO_2 \rightarrow \cdot SO_2^+ + e^-$$

$$2\ AlCl_4^- + \cdot SO_2^+ + SO_2 \rightarrow \cdot SO_3^- + SOCl_2 + 2\ AlCl_3$$

$$\underline{SO_3^- \rightarrow SO_3 + e^-}$$

$$2\ AlCl_4^- + SO_2 \rightarrow SO_3 + 2\ AlCl_3 \cdot SOCl_2 + 2\ e^-.$$

Both SO_2^+ [22] and SO_3^- [23] have been identified in the literature.

Confirmation of the SO_3 overdischarge product must include spectroscopic characterization of all $LiAlCl_4$ adducts with SO_2, $SOCl_2$, and SO_3. Control Raman spectra of SCl_2 and S_2Cl_2 in electrolyte will help confirm or deny their presence and the possibility of other oxidative pathways for anode limited overdischarge.

4.0 ELECTRON SPIN RESONANCE SPECTROSCOPY

4.1 EXPERIMENTAL

The details of the instrumentation for ESR are given in QRI. Electronic g factors have been corrected using α,α- diphenyl- β -picrylhydrazyl (DPPH) as a standard (g = 2.00365). Two scans were made with the DPPH signal on opposite sides of the field set. Using the known value for g, the correct magnetic fields were back calculated, and two simultaneous linear equations were set up to solve for correction factors for the observed field positions:

$$H = A\,(H_{OBS}) + B$$

The resulting values for A and B were: A = .963 and B = 96.3 gauss. Application of this correction to other DPPH scans produced the correct g to within $\pm$ 0.00002. Furthermore, application of this correction produced a more consistent set of g values for the discharged electrolyte yielding small enough rms deviations which convincingly separated the different resonances into discreet values.

The in situ cell previously described (QRI) was discharged producing the spectra in Figure 7. There is evidence of a substantial change in signal as the cell went into reversal at about 7:30 AM. This new resonance remained throughout anode limited overdischarge and for at least 12 hours following removal of the power supply. Thus, the technique in principle is viable but a number of factors conspired to produce uninterpretable spectra.

Firstly, the nickel electrodes possessed a degree of ferromagnetism so that a strong local field was created at the sample to shift the spectra in an unknown amount.

Secondly, the electrolyte-soaked carbon may have dominated most of the spectra. And thirdly, the cathode was apparently too large and withheld electrolyte from the separator paper at end of discharge producing an electrolyte limited condition and very high negative voltages during overdischarge due to the scarcity of electrolyte between the electrodes. These problems will probably be eliminated through use of platinum rather than nickel and carbon electrodes.

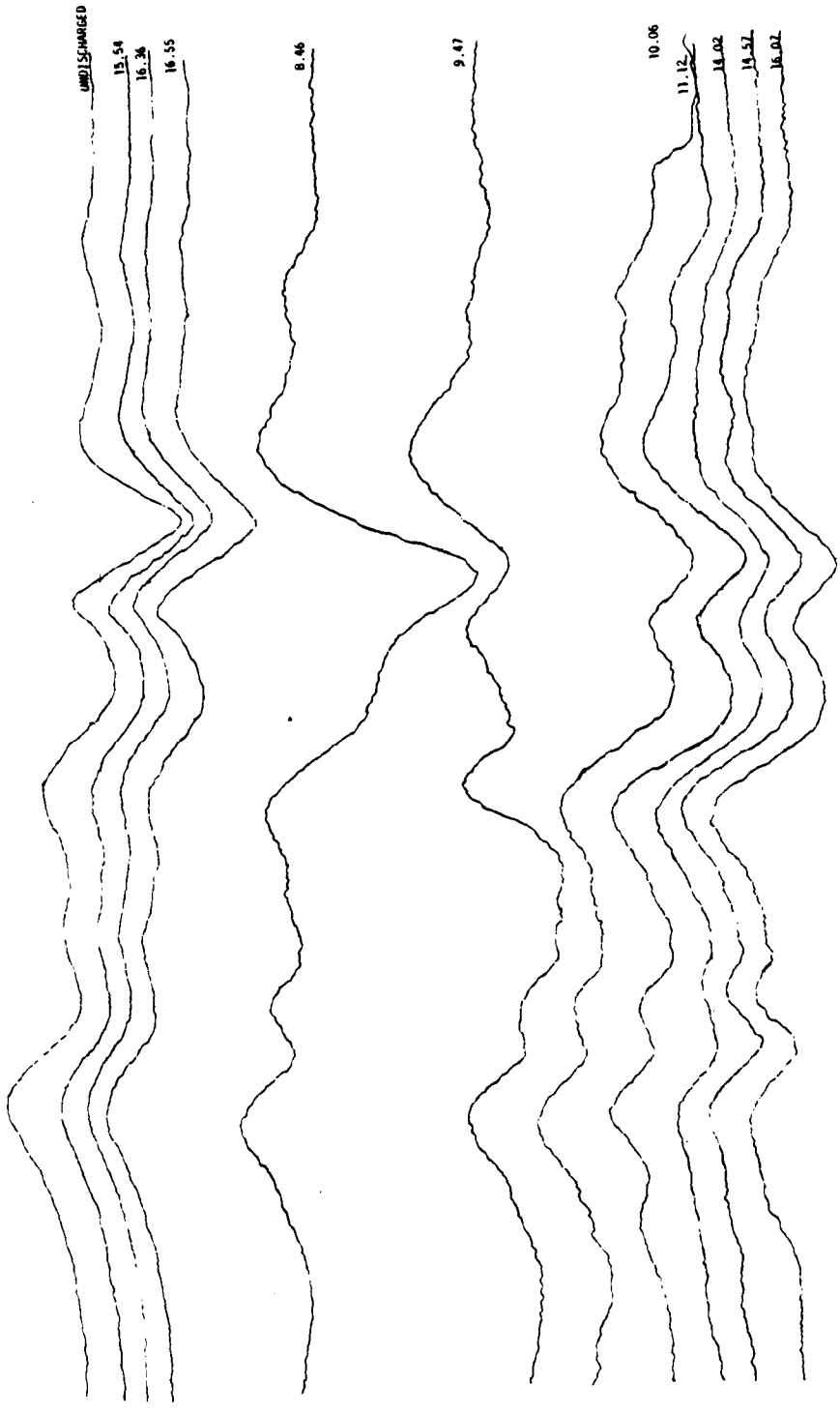

Figure 7. ESR Spectra of Discharging in situ Cell

4.2 RESULTS

Several control samples were scanned in quartz tubes in order to characterize electron spin resonance in known combinations of $Li/SOCl_2$ reactants and products. Electronic g factors are summarized in Table 6 along with root-mean-squared deviations where more than two spectra were recorded. LiCl alone produces a weak signal with splitting of 83.4 gauss due to crystal lattice or color center defects. Carbon with and without electrolyte produces a single strong resonance. The presence of electrolyte intensifies this resonance. Lithium produces a complex Dysonian resonance due to skin effects. Addition of electrolyte to the lithium results in a change in resonance shape due to the alteration of the metals surface with a passive film. Sulfur in electrolyte yields a single weak resonance. Electrolyte alone and SO_2 saturated electrolyte show no electron spin resonance. No signal was detected from the quartz tube alone.

A striking series of ESR resonances appear during discharge and overdischarge as shown in Figure 8. Although no resonance occurs in pure electrolyte, Species I ($g = 2.0149$) occurs already at 25 percent discharge. This species is stable indefinitely in the sample tubes. At 60 percent discharge, the sampled electrolyte also contains Species II ($g = 2.0027$). Over the course of several days, this second species begins to disappear in the sample tube while the first remains intact. By 100 percent discharge, the Species II resonance exceeds that of I, but within days, II disappears and I remains.

In cathode limited overdischarge, both I and II remain but are somewhat diminished in relative amplitude. Resonance I is also split with a very close resonance V, at $g = 2.01304$. With time, both II and V disappear.

Electrolyte from the 92 percent anode limited overdischarged electrolyte retains Species I alone which is stable on storage. However, the resonance for I tends to be more asymmetric and, by 150 percent overdischarge, two new resonances at $g = 2.01697$ and 2.00637 appear to replace I.

If solids are brought over from the discharged battery and included with the ESR spectrum of discharged or overdischarged electrolyte, resonance II is broadened upfield somewhat by the introduction of LiCl which resonates with $g = 2.00645$ (Table 6). Furthermore, the solid LiCl introduces hyperfine splitting. The extent of LiCl resonance can always be ascertained from the magnitude of the satellite peaks. The central LiCl resonance is considerably smaller (Figure 9). The signal for the carbon/TFE cathode, $g = 2.00437$, does not occur in any of the sampled electrolyte spectra.

TABLE 6
Corrected Electronic g Factors

	g	$\Delta(g^{1})$	$g_{\perp}$	$\Delta(g_{\perp})$	$g_{\parallel}$	$\Delta(g_{\parallel})$	g_{III}	$\Delta(g_{III})$	g_{IV}	$\Delta(g_{IV})$	g_{IV}
DPPH Solid AWP in THF Solution	2.00366	.00035									
Sulfur in Electrolyte			2.01517	-							
Cathode Mix With and Without Electrolyte	2.00437	.00046									
Lithium With and Without Electrolyte	2.00433[3]	.00026									
Lithium Chloride Crystals	2.00645	.00061									
25% Discharged			2.01442	-							
60% Discharged			2.01430	.00085	2.00212	.00085					
100% Discharged			2.01510	.00039	2.00247	-					
50% Cathode Limited Overdischarged			2.01509	.00055	2.00335	.00064					2.01304[2]
92% Anode Limited Overdischarge			2.01525	.00054							
150% Anode Limited Overdischarge							2.01697	.00023	2.00637	.00067	
Average			2.01498		2.00265		2.01697		2.00637		2.01304

[1] R.M.S. Deviation
[2] Estimated From Overlapping Signals
[3] Center of Complex Pattern

Strategic Systems Division
GTE Communications Products
Corporation

Figure 8. ESR Spectra

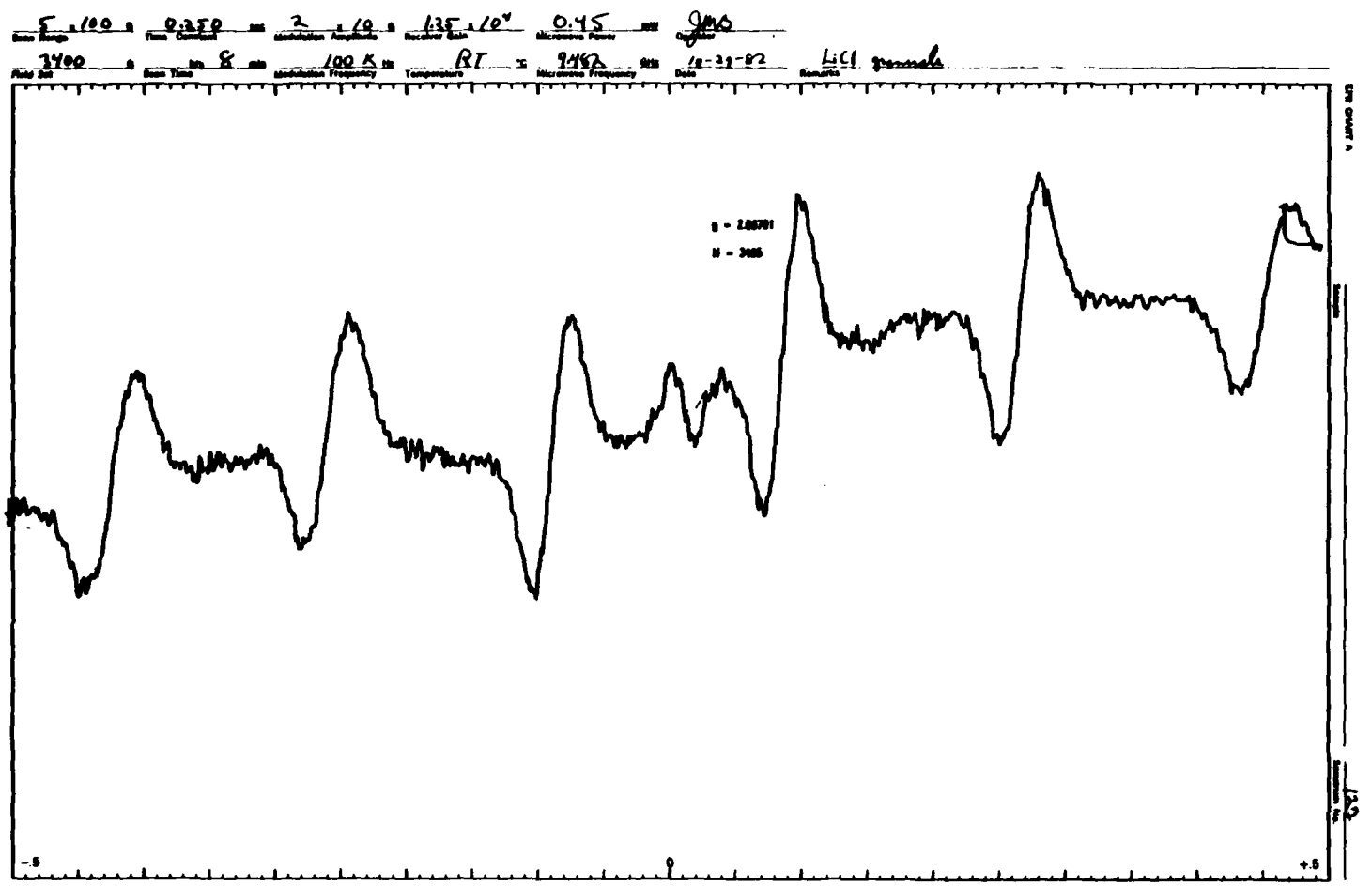

Figure 9. ESR Spectra of Solid Crystalline LiCl

Figures 10 and 11 show the effects of liquid nitrogen freezing of resonances I from 100 percent discharged and 92 percent anode limited overdischarged electrolyte, respectively. Though qualitatively the same, the anisotropic peaks fall at different positions, and the discharged resonance exhibits splitting with $\Delta H = 92$ gauss.

The ESR spectrum of discharged electrolyte is identical to that obtained by Carter et al[24] for frozen electrolyte with the addition of the frozen anode limited overdischarged electrolyte.

4.3 DISCUSSION

Electron Spin Resonances (ESR) occur in a surprising variety of substances connected with the $Li/SOCl_2$ cell. It is extremely important to recognize any artifacts not connected with the reaction mechanisms of interest, and so a number of controls were performed.

Incomplete reduction of acetylene during production of SAB evidently leaves the substance with a free radial. Addition of electrolyte enhances this signal. This strongly suggests a surface-absorbed complex is formed involving carbon, $\dot{S}OCl_2$, and perhaps $LiAlCl_4$, and may account for the anomalously high OCV (3.72 volts in some commercial cells) and long time required to develop full OCV. In any event, this signal would be expected to interfere in any in situ experiments with carbon cathodes.

ESR spectra of metals arises from resonance of conduction electrons but are strongly influenced by sample size, surface effects, impurities, and dislocations. Complete analysis of the complex spectra of lithium and lithium with electrolyte is outside the scope of this study, but it is clear that these resonances will interfere with in situ studies.

Sulfur is known to produce free radicals in the presence of oxidizing solutions such as sulfuric acid[25]. Sulfur in electrolyte is no exception, and its resonance corresponds closely with resonance I from discharged electrolyte. This probably represents a small amount of charged polymeric $(S_n)^+$ sulfur produced in discharge. An alternate choice would be a small percentage of S_8 rings which are known to open, forming diradicals ($\cdot S\text{-}S_6\text{-}S\cdot$).

The presence of an ESR resonance and splitting patterns from LiCl crystals (Figure 9) is probably due to dislocations since no radiation was used to produce color centers. It is therefore surprising that the electrochemically produced LiCl produced

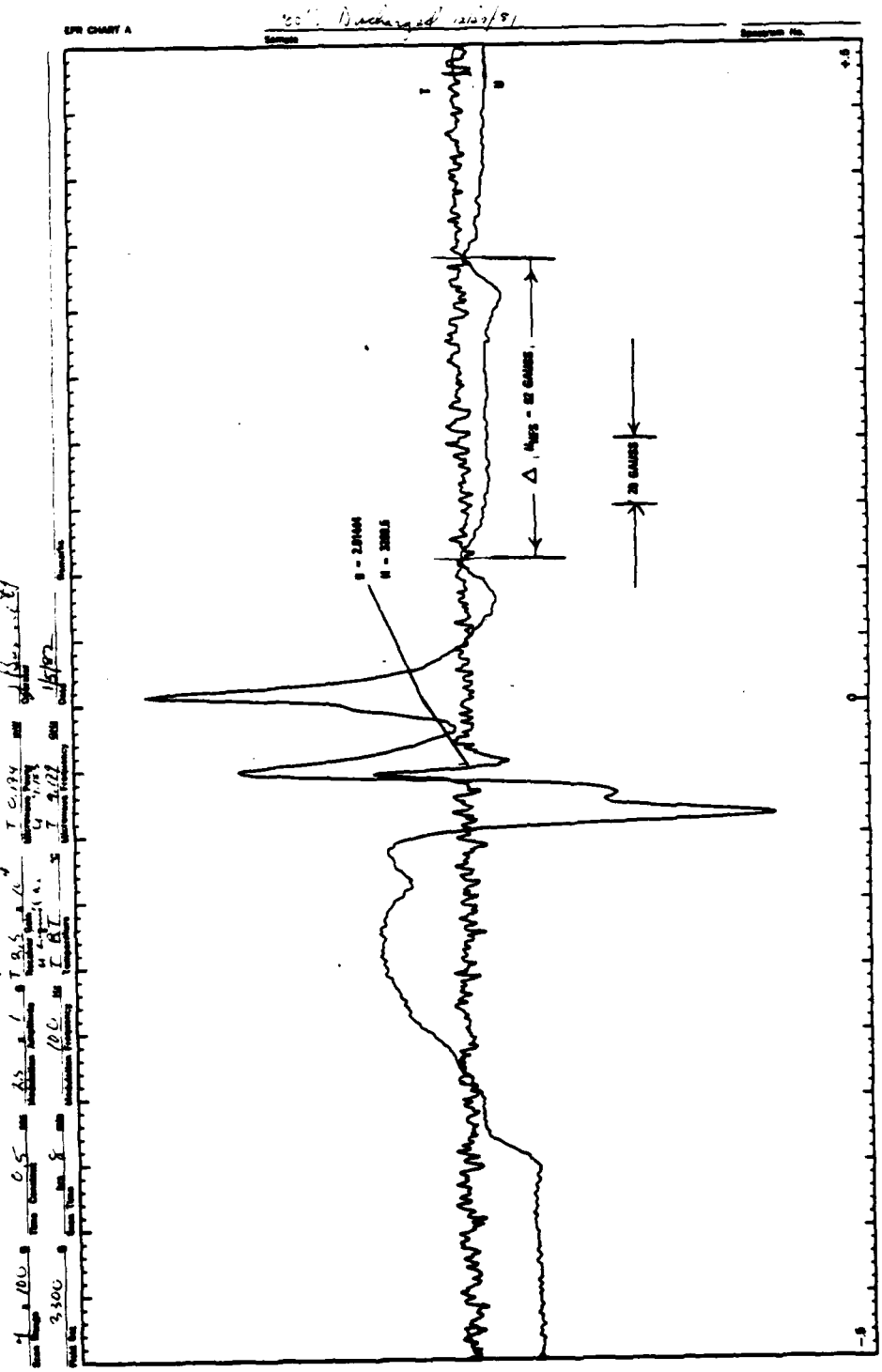

Figure 10. ESR Spectra of Liquid Nitrogen Cooled Electrolyte from Discharged Electrolyte

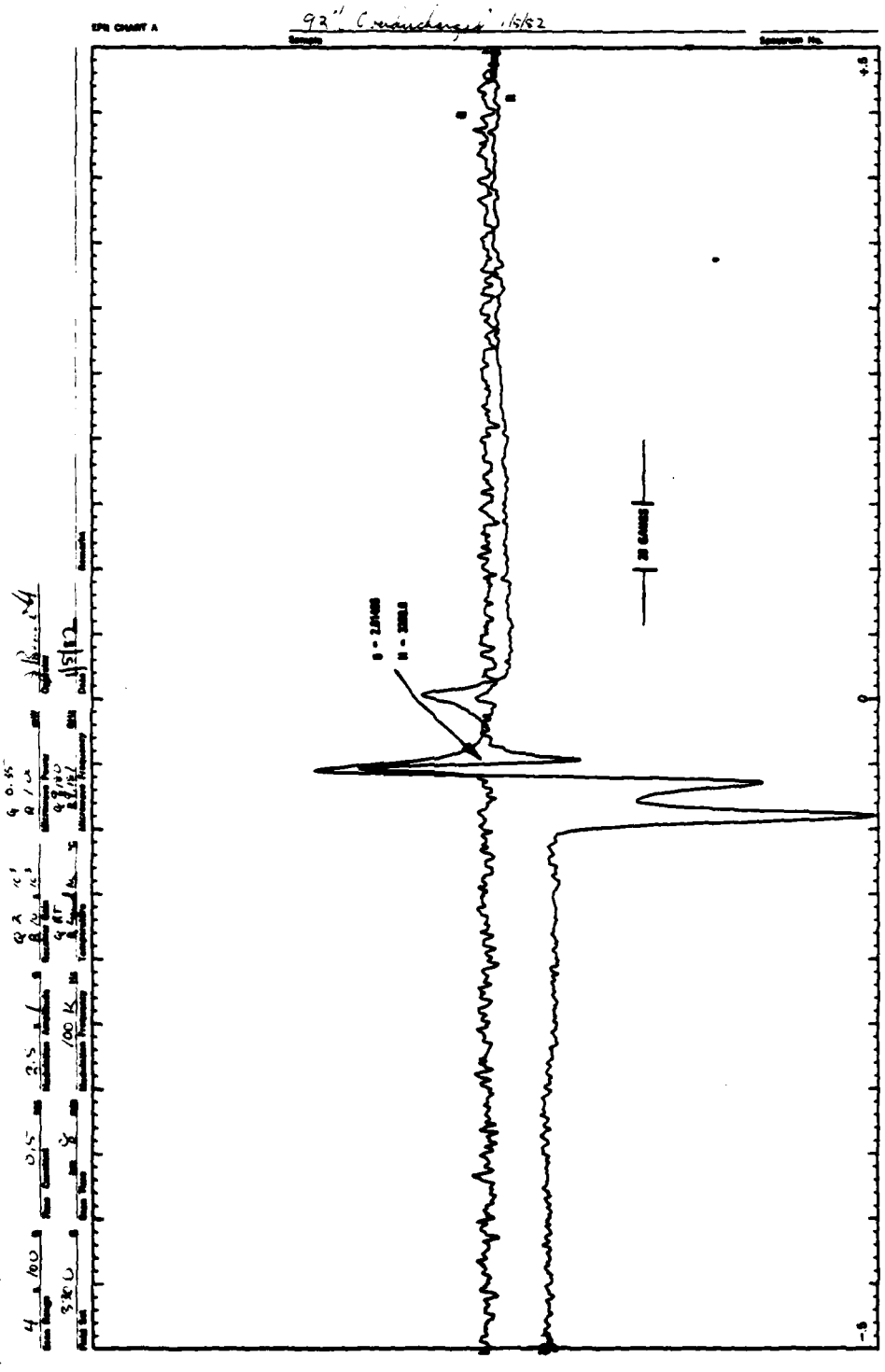

Figure 11. ESR Spectra of Liquid Nitrogen Cooled Electrolyte from Anode Limited Overdischarge Electrolyte

the same resonance and splitting. No explanation can be offered at this time but at least the signal is weak enough not to interfere with the other species. If the solids are allowed to settle out, the LiCl resonance and splitting disappear.

It is certain that Species I corresponds to charged sulfur which probably is a by-product of the sulfur formed in discharge though it may be an intermediate in the formation of sulfur. It is not unexpected because of the known tendency of elemental sulfur to oxidize. The quantity of I does not correlate with discharge so that a rather constant amount of I is present from the time that sulfur first makes its appearance at the beginning of discharge.

Species I resists reduction in cathode limited overdischarge and oxidation in anode limited overdischarge until 150 percent overdischarge, where I and II are evidently oxidized to Species III and IV.

Somewhere between 25 and 60 percent discharge, resonance II is detectable and increases with discharge, eventually becoming larger than resonance I. Species II resists reduction on cathode limited overdischarge but is eliminated probably through oxidation in anode limited reversal.

Species IV formed on excessive 150 percent overdischarge probably produces a resonance close to that of reduced SO_2 formed as follows:

$$SO_2 + e^- \rightarrow (SO_2^-)^-$$
$$(SO_2^-)^- + SO_2 \rightarrow (S_2O_4^-)^-$$

where the g for $(SO_2^-)^-$ is 2.00727 and g for $(S_2O_4^-)^-$ is 2.00607[26].

One may speculate about the relative oxidation potential of the five free radicals on the basis of their known lifetimes and behavior in anode and cathode limited overdischarge.

Finally, on anode limited overdischarge, Species IV appears evidently through oxidation on a bare nickel anode, but disappears again within 11 days.

On the basis of the observed free radical behavior on discharge, overdischarge, and storage, the species can be arranged in order of descending reduction potential

$$V > II > I > III$$

with the exception of LiCl which resonates as a defect solid. The stability of all five resonances with time in the discharged electrolyte media is approximately as follows:

$$I = III > II = IV > V.$$

5.0 MORPHOLOGICAL STUDIES

5.1 EXPERIMENTAL

The cell used to investigate dendrite morphology in cathode limited cells during overdischarge consisted of a single 3.0 x 3.5 cm Teflon-bonded carbon cathode 3.1 mm thick positioned between two 3.0 x 3.5 cm Li anodes. The cathode and two lithium anodes were parallel and separated 6 mm. The Li electrodes were fabricated by pressing two 0.76 mm sheets of Li foil on both sides of a 5 Ni 10 - 2/10 Exmet grid to which was welded a 0.76 mm dia Ni lead wire. Since the electrodes were held rigidly in place with the thick Ni lead wires, no separator was required, thus allowing an unobstructed view of all electrode surfaces. The cell was evacuated to $< 200\ \mu$ Hg then filled with 1.8M $LiAlCl_4/SOCl_2$ electrolyte. The cell together with the funnel, used for adding the electrolyte after evacuation, is shown in Figure 12.

The anode limited cells were constructed similarly to the cathode limited cells except the two Li electrodes measured 3.2 x 3.2 cm and were covered with a single layer of 0.025 cm thick Li (10 mil) instead of the two 0.76 mm thick sheets of Li per electrode used in the cathode limited design.

The optical microphotographs were taken with a Bausch & Lomb Stereo Zoom 7 microscope equipped with a 3-1/4 x 4-1/4 in. Polaroid camera. The scanning electron microscope (SEM) studies were carried out with a Japan Electron Optics Laboratory Co., Ltd., Model U-3.

To avoid the possible loss of oxygen sensitive reaction products such as lithium-carbon intercalation compounds, the overdischarged cell was disassembled in the dry room and the cathode was placed in a vacuum desiccator within one minute after removal from the $SOCl_2$ electrolyte. It was then vacuum dried ($<200\ \mu$ Hg) for 48 hours at 25°C. The Li dendrites were then scraped from a small piece of the cathode broken off inside an argon-filled glove box (<60 ppm H_2O). The piece of carbon was next ground in a mortar into a fine powder to fill a 0.3 mm ID quartz capillary for the Debye-Scherrer X-ray diffraction analysis. The diffraction patterns were obtained using CuKα radiation from a Phillips X-ray generator with a Ni filter operated at 40 kV and 20 mZ and a 115 mm diameter Debye-Scherrer camera (Phillips). An eight-hour exposure was taken using high-speed reflex 25 double coated film (Ceaverken AB, Sweden).

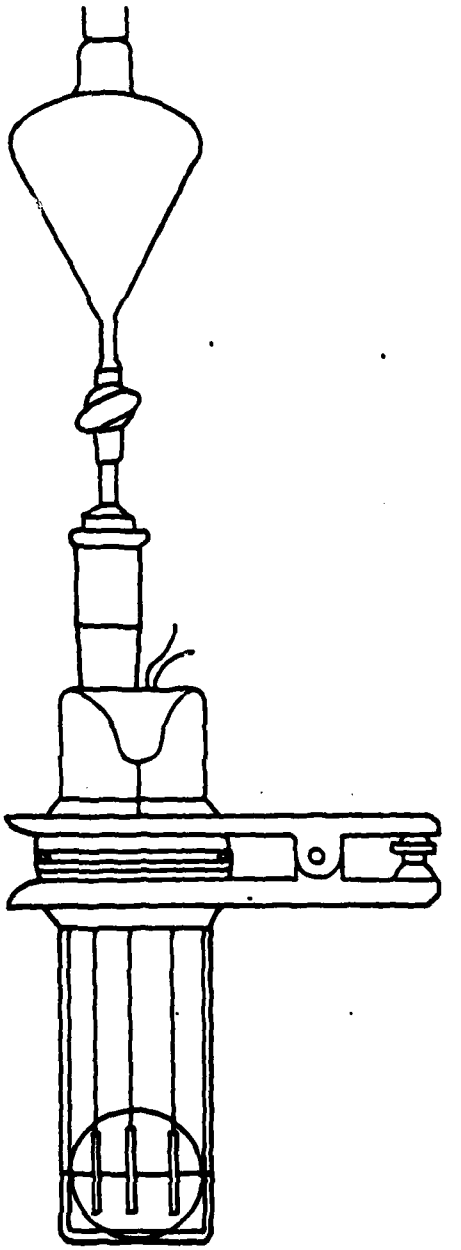

Figure 12. Glass Cell for in situ Microphotography of Lithium Dendrites

Other small portions of the cathodes, on which the lithium dendrite deposits had not been disturbed, were mounted using 3-M Co. copper conducting tape on 25 mm diameter brass studs inside an argon glove box so that the samples could be transferred into the SEM while in an inert atmosphere.

The experimental overdischarge test conditions are summarized in Table 7.

TABLE 7
OVERDISCHARGE CAPACITIES AND TEST CONDITIONS FOR LITHIUM DEPOSITION INVESTIGATION

Limiting Electrode+	Temp (°C)	Current Density (mA/cm^2)	Capacity to 0.0V (mAh/cm^2)	Over Discharge Capacity (mAh/cm^2)
C	25	5	58.5	24
C	25	2	372	55.8
C	25	20	113	85.9
C	-40	1 5*	234	59
C	-40	10**	253	105.
C	40	2	300	64
C	40	20	77.4	89
A	25	2	102	274
A	25	20	60	127

+*Cathode and anode limited cells are designated C and A, respectively.*

*The cell was discharged at -40°C at .050 mA/cm^2 constant current then overdischarged at 1.5 mA/cm^2.

**The cell was discharged at -40°C at 1.0 mA/cm^2 to 0.00V then overdischarged at 1.0 mA/cm^2 for 24.2 mAh/cm^2 then an additional 81.3 mAh/cm^2 at 10 mA/cm^2.

5.2 RESULTS AND DISCUSSION

5.2.1 Overdischarge of Cathode Limited Cells at 25°C

Three cathode limited $Li/SOCl_2$ cells were overdischarged at 25°C at 2,5, and 20 mA/cm^2. The capacities obtained on discharge to reversal and the capacities to which the cells were intentionally overdischarged are listed in Table 7. The cell tested at 5 mA/cm^2 used a 0.96 mm thick cathode compared to the 3.1 mm thick cathode used for the cells discharged at 2 and 20 mA/cm^2. The thin 0.96 mm cathode was only used for the first test to evaluate the cell for the in situ microphotography. All later tests were carried out with the thicker 3.1 mm cathodes to allow easier sampling of carbon from the interior of the cathode.

For the cell discharged at 5 mA/cm^2, the polarity of the cell reversed so that the cathode reached a maximum potential of -210 mV versus the Li anode. After 2.4 hours of overdischarge (24 $mAhr/cm^2$) the current was stopped to avoid a short circuit because the Li dendrites on the cathode almost reached the Li anode. Thus, it was only possible to overdischarge the cell 41 percent. During overdischarge, the cell potential rose from -210 mV to -120 mV most likely because the growth of dendrites on the carbon surface gradually increased the area of Li substrate available for Li deposition and decreased the distance between the growing dendrites and the Li electrode.

Figures 13 to 22 show various aspects of the carbon electrode overdischarged at 5 mA/cm^2 viewed face on and in cross section under an optical microscope (Figures 13 through 17) and with a scanning electron microscope (SEM) (Figures 18 through 22). Figure 13 gives an overall view of the top of the electrode at 5X magnification which is helpful in locating the position of later microphotographs at higher magnification. The Ni lead which was mostly covered with dendrites but smooth near the top can be seen in the upper part of Figure 13. The upper part of the Ni lead was free from dendrites because it was above the surface of the electrolyte. The contrast between the parts on the Ni lead which are smooth and those covered with Li deposits give a clear indication of the thickness of the deposits.

Figure 14 shows the area in the center of Figure 13 at twice the magnification (i.e., 10X vs. 5X magnification). Figure 15 shows the Li dendrite deposits on the surface of the carbon electrode at 30X magnification at a point slightly below center in Figure 14 and slightly at the left. Both white and grey Li dendrites can be seen in Figure 14 and 15. Later SEM observations showed that both types of deposits are Li but the white deposits have a thin coating of Li salts (e.g., $LiAlCl_4$ or possibly LiCl).

Figure 16 shows the Li dendrite encrusted lead as it meets the Exmet grid at 10X magnification compared to only 5X in Figure 13. Figure 17 shows a cross section of the 1 mm thick cathode at a magnification of 50X. Lithium dendrites on the surface of the cathode are clearly visible but no Li deposits were observed in the interior of the cathode when many samples were examined. The large bright particles seen at the top of Figure 17 and the smaller particles seen in the interior were introduced when the cathode cross section was cut.

Figure 18 is an SEM photograph of a cross section of the overdischarged cathode at a magnification of 160X seen at an angle of approximately 30°. The Li deposits on the surface of the electrode are seen, as well as two Li particles loosely attached to the

Figure 13. Lithium Dendrites on Carbon Cathode and the Exposed Exmet Grid and Lead (5X Magnification)

Figure 14. Lithium Dendrites on Carbon Cathode and Exposed Exmet Grid Directly Below the Lead (10X Magnification)

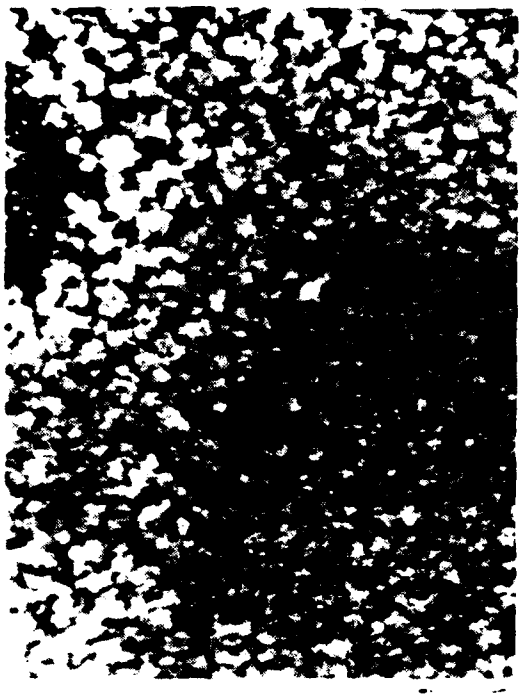

Figure 15. Lithium Dendrites on Carbon Cathode Surface (30X Magnification)

Figure 16. Lithium Dendrites on Lead and Exmet Grid Above Cathode (10X Magnification)

Figure 17. Optical Microphotograph of Cathode Cross Section (50X Magnification)

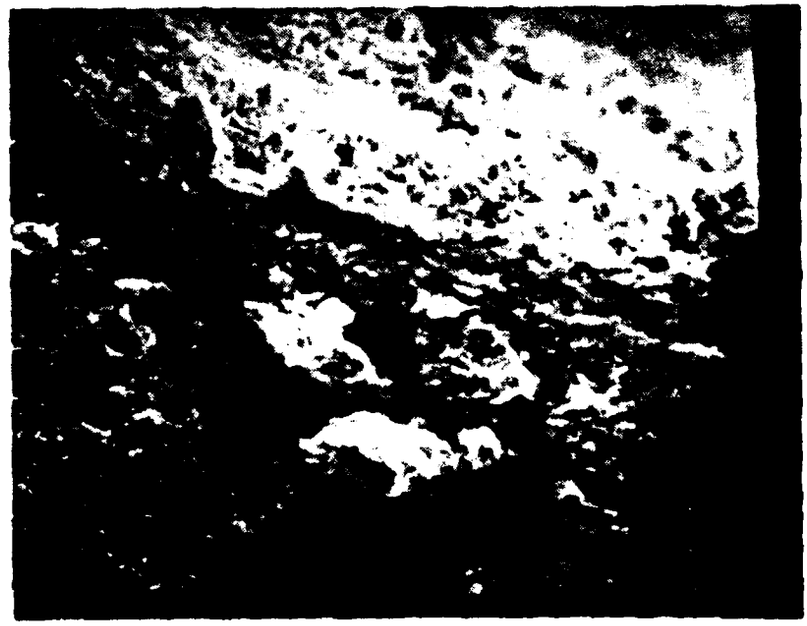

Figure 18. Scanning Electron Microscope Photograph of Cathode Cross Section (160X Magnification)

interior cross section, which again appear to be fragments from when the cross section was cut. A close examination of the clean cut carbon surface of the cross section shown in Figure 18, as well as several other places along the cross section, revealed no signs of Li deposition inside the cathode. In order for lithium to form by electrochemical reduction, contact between lithium and carbon must exist at least at the surface of the carbon electrode in order to provide an uninterrupted electronic path as the dendrites grow.

Figure 19 shows an SEM photograph of the Li dendrites on the surface of the overdischarged carbon electrode as seen at 50X magnification. The SEM photograph, as expected, is similar to the optical photograph of the cathode as shown in Figure 15 but shows somewhat more detail since the magnification was increased from 30X to 50X. Figure 20 shows a small portion from the center of Figure 19 with the magnification increased to 300X. Third in this series, Figure 21 shows a small portion from the center of Figure 20 with the magnification increased from 300X to 1000X. The coiled spaghetti-like structure of the Li filaments, which make up the Li nodules on the surface of the carbon electrode, is a remarkable structural feature of considerable practical importance. For example, since the nodules are porous and not solid, it is likely that they would not cause a serious short circuit problem in overdischarged cells. Furthermore, the small diameter of the Li filaments (i.e., $4 \cdot 10^{-3}$ mm) suggests that the filaments could easily grow through a glass fiber separator but could not carry significant currents should a short circuit occur when the dendrite grew to touch the Li electrode.

Figure 22 shows a SEM photograph of Li dendrites growing on the Ni lead wire at 1000X magnification. The Li dendrite structure on the Ni lead appears to be almost entirely of filaments without the plates or crystals seen in the nodules grown on the carbon surface. It is thought that the dendrites grown on Ni are almost entirely filaments because nucleation of Li dendrites occurs more easily on Ni than carbon, with fewer better-formed dendrites.

When interpreting the microphotographs of Li dendrites, it should be kept in mind that in solution the Li filaments are supported by the electrolyte and the dendrites are somewhat less compacted than in the photographs. Thus, they are much more porous and less able to support short circuit currents than the microphotographs would tend to suggest.

The high surface area of Li dendrites is of some concern since it could be the basis of a rapid reaction between the Li dendrites and discharge products such as elemental sulfur.

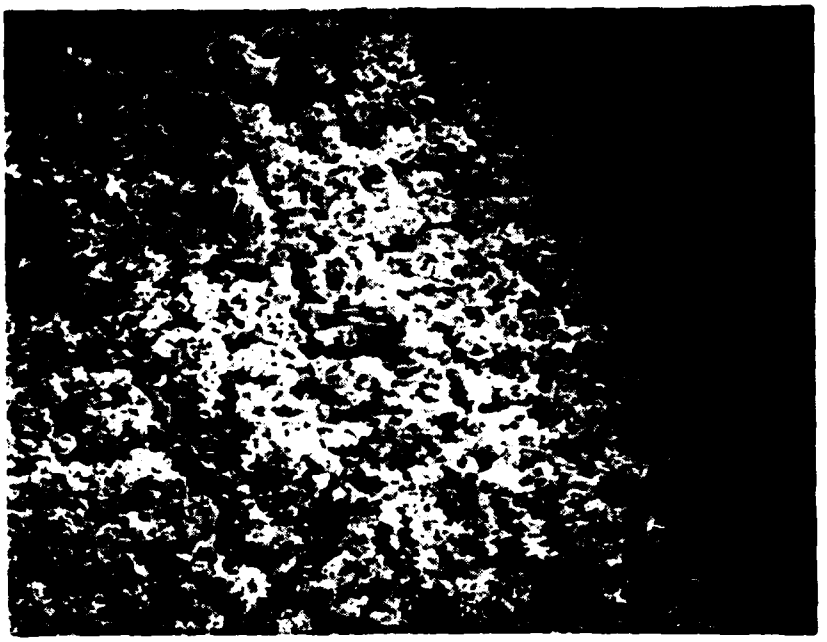

Figure 19. Scanning Electron Microscope Photograph of Lithium Deposits on Cathode Surface (50X Magnification)

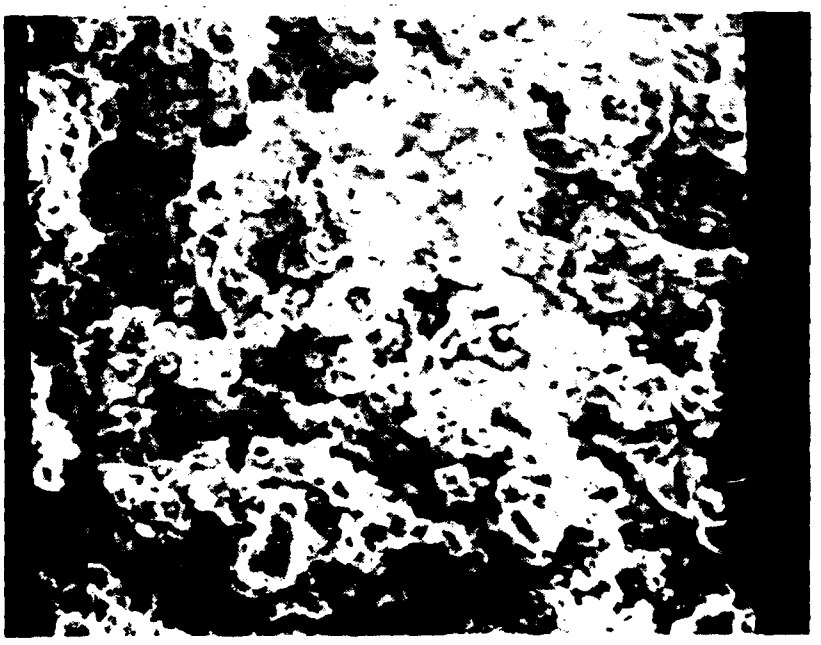

Figure 20. Scanning Electron Microscopeosits on Carbon Cathode Surface (300X Magnification)

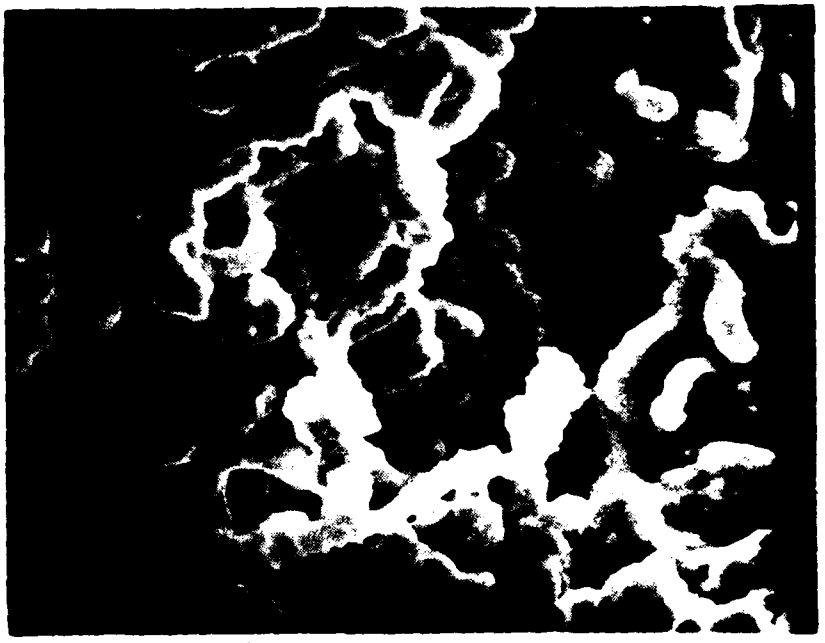

Figure 21. Scanning Electron Microscope Photograph of Lithium Dendrites on Carbon Cathode Surface (1000X Magnification)

Figure 22. Scanning Electrone (1000X Magnification)

5.2.1.1 Overdischarge at 2 mA/cm^2, 25°C

With the completion of the exploratory overdischarge study at 5 mA/cm^2 with a thin cathode, the first overdischarge test at 2 mA/cm^2, 25°C with a cathode limited cell with a 3.1 mm thick cathode was undertaken. In addition to in situ microphotographs of the lithium dendrites, the study included scanning electron microscope (SEM) examination of the dendrites and X-ray diffraction analysis of the carbon from the interior of the cathode. Microphotographs were also taken during long term storage to determine whether dendrite shape changes were taking place through a process of Ostwald ripening.

In principle, over a period of days or even weeks, small Li dendrites could undergo the process of Ostwald ripening[27, 28] during which small dendrites could dissolve and larger dendrites could grow. In overdischarged batteries, this process could lead to sudden unpredictable short circuits during storage resulting in thermal runaway and explosions.

To study Ostwald ripening of Li dendrites, a Li/$SOCl_2$ cell with a 3.0 x 3.0 x 0.317 cm carbon cathode positioned between two 3.0 x 3.5 cm x .152 cm Li anodes was constructed. The cathode contained 0.857g of Teflon-bonded carbon mix with a 5 Ni 10-2/0 Exmet grid in the center of the sheet without any grid edges exposed to the electrolyte which could stimulate dendrite growth. The cell was discharged at 2 mA/cm^2 at 25°C to a capacity of 372 mAhr/cm^2 at which time reversal occurred. The cell was then overdischarged 14.6 percent for an additional 55.8 mAhr/cm^2. During overdischarge, the cathode potential slowly rose from -0.180 to -0.126V with respect to the Li anode.

When the current was terminated at the end of overdischarge, Li dendrites extended at one point 7 mm from the surface of the carbon cathode towards the Li anode. Microphotographs of the dendrites were then taken at 3.8 and 15.2X magnification through a flat optical glass window in the side of the cell. Photographs were taken immediately at the end of overdischarge and after 15 and 21 minutes and 4, 16.2, 42, and 331 hours of 25°C storage.

Figures 23 and 24 show the Li dendrites on the carbon electrode after 21 minutes and 16.2 hours on open circuit. No shape change was observed to within $\pm$ 0.02 mm during not only the first 16.2 hours on open circuit but up to 331 hours, when the experiment was voluntarily terminated. The left portion of Figure 24 showing the small dendrites on the edge of the electrode is very dark because the left side was not illuminated as well as in Figure 23. The large mass of dendrites on the right-hand side of the

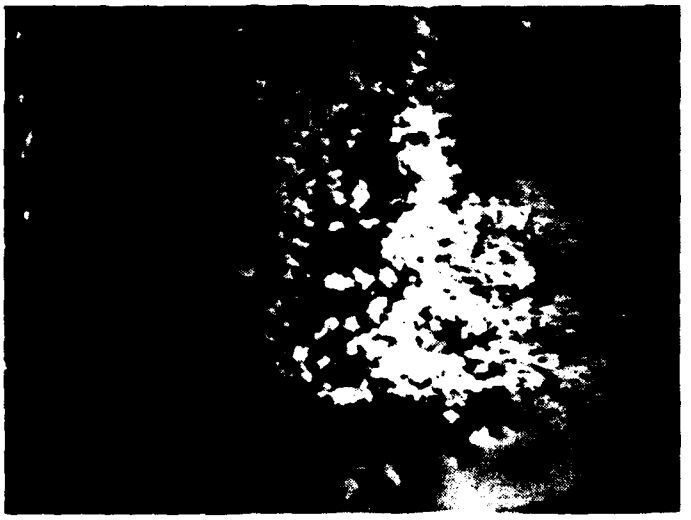

Figure 23. Lithium Dendrites on Overdischarged Cathodes on Open Circuit, 2 Sec Exposure

Figure 24. Lithium Dendrites on Overdischarged Cathode (3.8X Magnification); 16.2 Hours on Open Circuit 1 Sec Exposure

photographs extends about 7 mm from the electrode surface into the electrolyte. All the microphotographs were taken through the flat glass window in the cell while the electrodes were totally immersed in 1.8M $LiAlCl_4/SOCl_2$ electrolyte.

Figure 25 which shows the Li dendrites after 42 hours on open circuit shows the first significant effects of 25°C storage on the appearance of the dendrites. Although no shape change occurred, the dendrites turned from a bright silvery color to dull grey. Because of the loss of reflectivity, the exposure time for the microphotographs had to be increased from 2 to 5 seconds for Figure 25. The scattered white specs seen on the dendrites to the right side of the electrode in Figure 25 are small portions of the Li dendrites which have retained their original shiny metallic luster.

Earlier scanning electron microscope investigations have shown that Li dendrites deposited at 25°C at 5 mA/cm^2 have a coiled spaghetti-like structure made up of filaments with a diameter of $4X\ 10^{-3}$ mm. It is likely that the small pieces of lustrous uncorroded Li seen in Figure 25 are pieces of these filaments which have become electrically isolated from the carbon electrode and therefore have undergone less anodic dissolution, thereby avoiding formation of a thick grey secondary LiCl film. The presence of finely divided electrically isolated metallic lithium, 42 hours after the end of overdischarge, could lead to safety problems, such as casual explosions, should a cell undergo vibration and the Li dendrites break off and form a short circuit. Mixtures of finely divided carbon and lithium could be formed by vibration which could react to form excessive heat by forming in effect a multitude of tiny short-circuited cells.

Figure 26 shows the Li dendrites after 331 hours of open circuit storage. The Li dendrites had turned from the dull grey color observed after 42 hours of storage to a highly reflective white color which suggests that they were coated with a much thicker layer of LiCl. Microphotographs taken at 20X magnification tend to support this conclusion since the very fine structure of the dendrites observed after 16 hours tends to be obscured. At the present time, it is not known whether the Li dendrites have been completely or only partially converted to LiCl after 331 hours of 25°C storage.

The carbon-limited cell used for the Ostwald ripening study was overdischarged an additional 9.18 percent at 2 mA/cm^2, 25°C (i.e., 34.4 $mAhr/cm^2$ at the end of the 331 hour storage period after the old dendrites were shaken off. The Debye-Scherrer X-ray diffraction results for the carbon sample from the overdischarged cathode are shown in Figure 27 and the results compared with the known patterns for LiCl, rhombic sulfur, and Li_2O_2 are listed in Table 8. Similar comparisons for patterns from the literature for

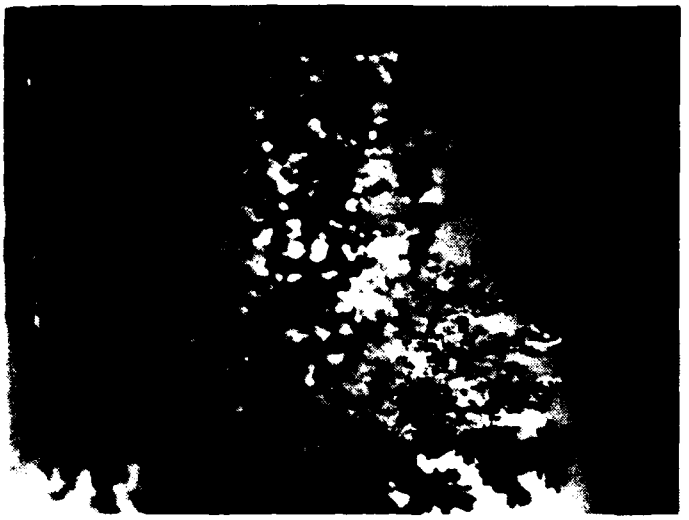

Figure 25. Lithium Dendrites on Overdischarged Cathode (3.8X Magnification); 42 Hours on Open Circuit, 5 Sec Exposure

Figure 26. Lithium Dendrites on Overdischarged Cathode (3.8X Magnification); 331 Hours on Open Circuit, 2 Sec Exposure

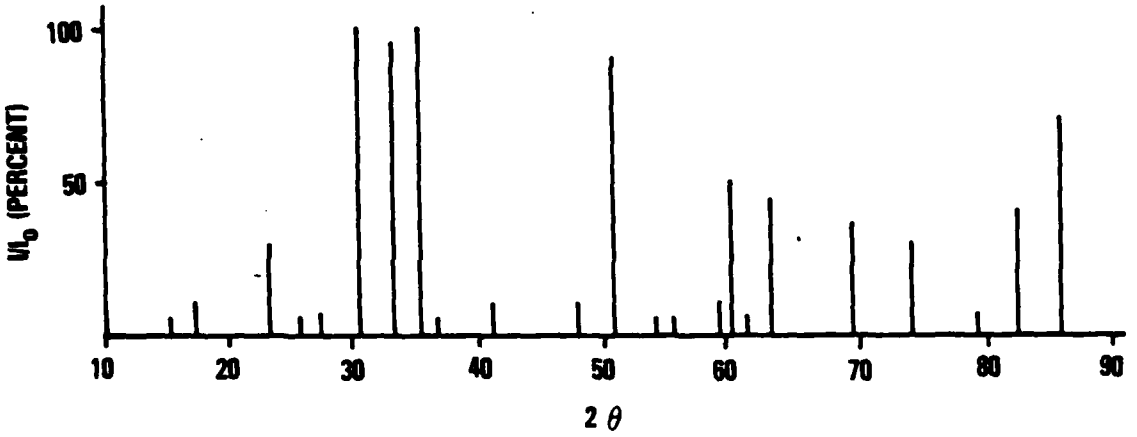

The carbon cathode was overdischarged 34.4 mAh/cm^2 (9.18%) at 2 mA/cm^2, 25°C.

Figure 27. Intensities of X-Ray Diffraction Pattern of Carbon From an Overdischarged Cathode.

Li_2S, Li_2O, $C_{16}Li$, $C_{40}Li$, C_6Li, $C_{12}Li$[29], and graphite intercalation compounds were also carried out. It was concluded that the overdischarged cathode contains only LiC1 and perhaps some rhombic sulfur and Li_2O_2. Thus, possibly hazardous reactions caused by the formation of metallic lithium, or lithium carbon intercalation compounds in the interior of carbon cathodes during overdischarge, appear remote. No plausible mechanism can be offered for the formation of Li_2O_2 as yet.

TABLE 8
DEBYE-SCHERRER X-RAY DIFFRACTION ANALYSIS OF CARBON FROM CATHODE OVERDISCHARGED AT 2 mA/cm² at 25°C*

Experimental Values					Literature Values			
Carbon Sample			LiCl		S Rhombic		Li_2O_2	
d (A)	2∂	I/I_o	d (A)	I/Io	d (A)	I/Io	d (A)	I/Io
5.80	15.26	5			5.46	60		
5.10	17.36	10						
3.80	23.4	30			3.89	100	3.81	60
3.45	25.80	5						
3.25	27.42	5			3.12	80		
2.94	30.38	100	2.967	100				
2.70	33.16	95			2.71	100	2.72	80
2.55	35.16	100	2.570	86			2.561	100+
2.45	36.66	5						
2.20	41.00	10			2.21	40	2.22	80
1.90	47.82	10			2.026	80	1.916	30
1.80	50.68	90	1.817	58			1.875	60
1.70	53.88	5						
1.66	55.30	5					1.572	100
1.56	59.18	10	1.550	29				
1.54	60.00	50						
1.51	61.34	5						
1.475	62.96	45	1.484	16				
1.35	69.58	35			1.352	60	1.335	80
1.275	74.34	30					1.283	40
1.205	79.46	5						
1.17	82.34	50	1.179	10				
1.145	85.56	70	1.149	12				
1.045	94.96	50	1.0491	8			1.02	70
			0.9892	9				

*All diffraction results were obtained using CuKα radiation with a Ni filter.

5.2.1.2 Overdischarge at 20 mA/cm^2, 25°C

The cell potentials during discharge are shown in Figure 28. The discharge capacity to 0.0V was 1.014 Ahr and 1.787 Ah at the end of overdischarge when the current was voluntarily terminated and microphotographs taken of the dendrites. Based on the 1.014 Ahr to 0.00V obtained at 20 mA/cm^2, the cell was 76.2 percent overdischarged. However, when a similar cell was discharged at 2 mA/cm^2 at 25°C, a capacity of 3.37 Ah was obtained. Thus, calculated on the basis of the nominal capacity at 2 mA/cm^2, the overdischarge was only 22.9 percent. Since it is the number of coulombs of overdischarge which determines the amount of lithium deposited on overdischarge, the nominal cathode capacity is the preferred base capacity when calculating the amount of overdischarge.

A microphotograph (3.8X magnification) was taken of the Li dendrites at the end of the overdischarge period. The dendrites were similar to those observed at 2 mA/cm^2, 25°C and discussed in detail earlier.

The X-ray diffraction peaks obtained for the carbon sample from the cathode discharged at 20 mA/cm^2, 25°C are listed in Table 9. The diffraction pattern shows the peaks only for LiCl and not for rhombic sulfur as just reported for the cell overdischarged at 2.0 mA/cm^2 at 25°C. It is known from the literature[30] that the $SOCl_2$ discharge intermediate is stable for several days before decomposing into sulfur and SO_2; thus, it is likely that sulfur was not found in the cathode of the cell discharged at high rate because the $SOCl_2$ intermediate did not have sufficient time to decompose. Furthermore, the X-ray diffraction technique has a detection sensitivity of only five percent and the cell contained 200 ml of electrolyte permitting the dissolution of a large amount of sulfur.

Examination of the surface of the cathode at 1000X and 300X magnification using a scanning electron microscope (SEM) revealed that the nodular dendritic Li deposits were made up of Li filaments with a diameter of 4X 10^{-3} mm. Since the Li filaments are of the same diameter as the deposits seen earlier on cathodes overdischarged at 2 mA/cm^2, it was concluded that the diameter of the Li filaments is not influenced by the current density from 2 to 20 mA/cm^2.

Cross sections of the cathode overdischarged at 20 mA/cm^2 were examined at 30X magnification under an optical microscope at at 40, 300, and 1000X using the SEM. No signs of electrodeposited Li in the interior of the cathode were observed. Eight SEM photographs were taken and are on file.

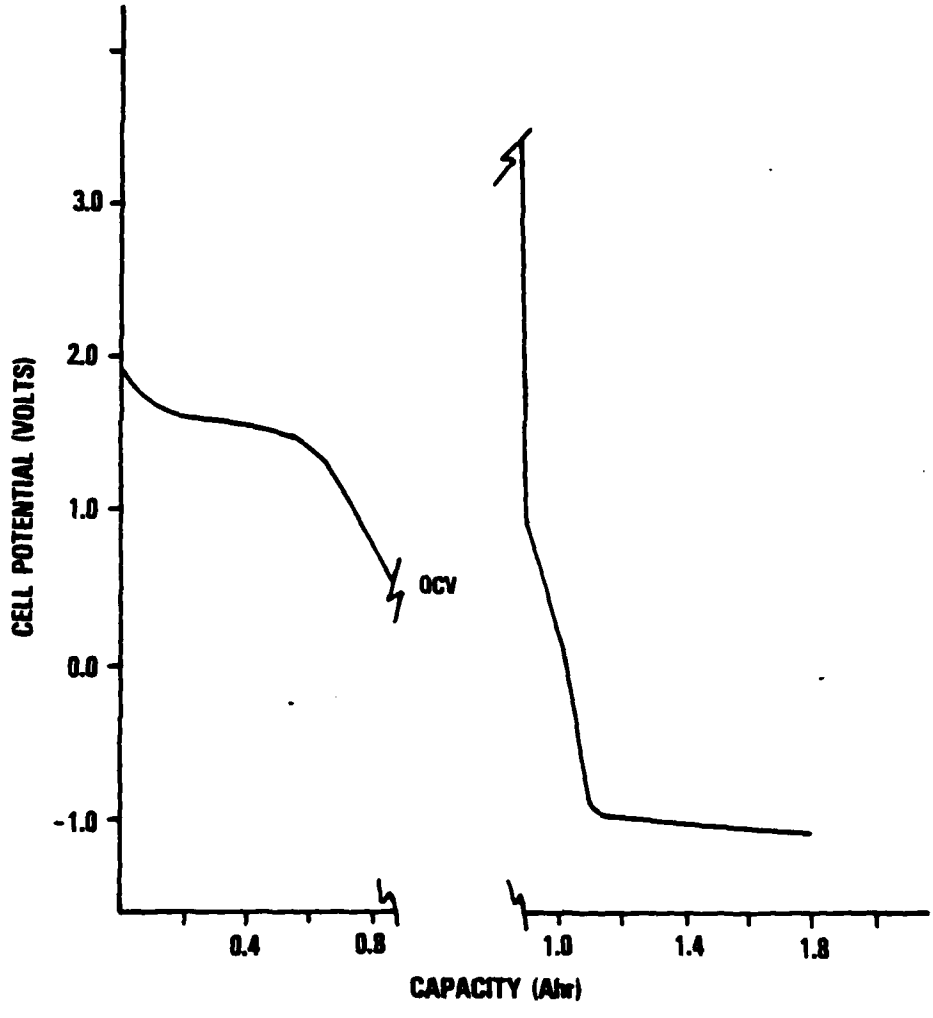

The cell was discharged to 0.52V, then left on open circuit for 16.5 hr when the discharge was resumed. The cathode was 3.0x3.0x0.32cm.

Figure 28. Behavior of a Cathode Limited Li/$SOC1_2$ Cell During Discharge and Overdischarge at 20 mA/cm^2 at 25°C.

TABLE 9
DEBYE-SCHERRER X-RAY DIFFRACTION ANALYSES OF CARBON FROM CATHODE OVERDISCHARGED AT 25 and -40°C*

Cell Discharged at 25°C, 20mA/cm^2			Cell Discharged at -40°C, 1.5 mA/cm^2		
d (A)	2θ	I/Io	d (A)	2θ	I/Io
			5.90	15	5
			5.20	17.04	10
			3.85	23.08	90
			3.68	24.16	30
			3.45	25.84	50
			3.28	27.16	50
2.95	30.26	100	2.97	30.06	100
			2.73	32.78	100
2.55	35.16	100	2.57	34.88	100
			2.44	36.80	10
			2.31	38.96	30
			2.22	40.60	50
			2.05	44.14	10
			1.99	45.54	5
			1.92	47.30	70
			1.87	48.64	20
1.81	50.36	100	1.82	50.08	90
1.54	60.02	90	1.78	51.28	5
1.475	62.96	50	1.72	53.20	30
1.278	74.12	10	1.69	54.22	30
			1.57	58.76	90
			1.54	60.02	90
			1.485	62.48	50
			1.435	64.92	5
1.173	82.08	30	1.358	67.58	50
1.144	84.64	50	1.285	73.66	50
1.044	95.08	50	1.215	78.68	50
0.984	103.0	45	1.18	81.50	50
			1.15	84.10	50

*All diffraction results were obtained using CuKα radiation with a Ni filter.

5.2.2 Overdischarge of Cathode Limited Cells at -40°C

A carbon limited cell with 3.0 x 3.0 cm cathode containing 0.877 g of carbon was discharged at 0.5 mA/cm^2 at -40°C instead of 2.0 mZ/cm^2 because the cell polarized to -0.65V after 5.37 minutes at the higher current density.

The cell potentials during discharge at 0.5 mA/cm^2 and overdischarge at 1.5 mA/cm^2 are shown in Figure 29. The cell discharged for 213.8 hours delivering 234 mAh/cm^2 to a 0.0 V cut-off after which it was overdischarged 59 mAh/cm^2 for a total capacity of 293 mAh/cm^2. A similar cell discharged at 25°C at 2 mA/cm^2 delivered 372 mAh/cm^2 to a 0.0 V cut-off, thus, the cathode in principle was only 63 percent depleted at -40°C. Based on the nominal capacity at 2 mA/cm^2 at 25°C, the cathode tested as -40°C at 1.5 mA/cm^2 was 15.9 percent overdischarged.

The overdischarge at -40°C was terminated voluntarily and the cell was immediately transferred from the refrigerated chamber to the dry room. Even in the dry room, frost formed on the cell window making photography of the Li dendrites difficult for about 20 minutes until the cell warmed up above the dew/frost point (i.e., -20°C at 4.1 percent R.H.). A series of 14 microphotographs at 3.8X magnification were taken of the Li dendrites on the cathode through the cell window during the period from 23 to 118 minutes after the end of overdischarge. The cell was then drained of electrolyte, disassembled, and the cathode placed in a vacuum desiccator for approximately 70 hours to remove all $SOCl_2$ prior to X-ray and SEM studies.

The optical microphotographs show that the Li dendrites formed at -40°C at 1.5 mA/cm^2 are similar in appearance to those formed at 25°C at 2 mA/cm^2. Two SEM photographs of Li deposits on the cathode surface at 100 and 300 X magnification do not reveal the Li nodules made up of Li filaments as observed at 25°C. The absence of these features was most likely caused by the dendrites being broken off close to the carbon surface when the cell electrolyte was drained after two hours of 25°C storage immediately after -40°C overdischarge.

Cross sections of the cathodes overdischarged at -40°C at 1.5 mA/cm^2 were examined at 40X and 300X magnification by SEM and two microphotographs were taken. No signs of electrodeposited Li in the interior of the cathode were observed.

The X-ray diffraction peaks obtained for carbon from the cathode overdischarged at -40°C, 1.5 mA/cm^2 are listed in Table 9. A preliminary analysis of these results indicates that the cathode contained LiCl, Li_2O_2, and rhombic sulfur.

The cathode limited cell which was overdischarged at -40°C, 10 mA/cm^2 contained 0.762g of carbon and was of the same design as used earlier.

The cell potentials during discharge and overdischarge at -40°C are shown in Figure 30. The cell was discharged at 1.0 mA/cm^2 then overdischarged at 1.0 mA/cm^2 for 24.2 mAh/cm^2 before the current was increased to 10 mA/cm^2. Because of the reduced

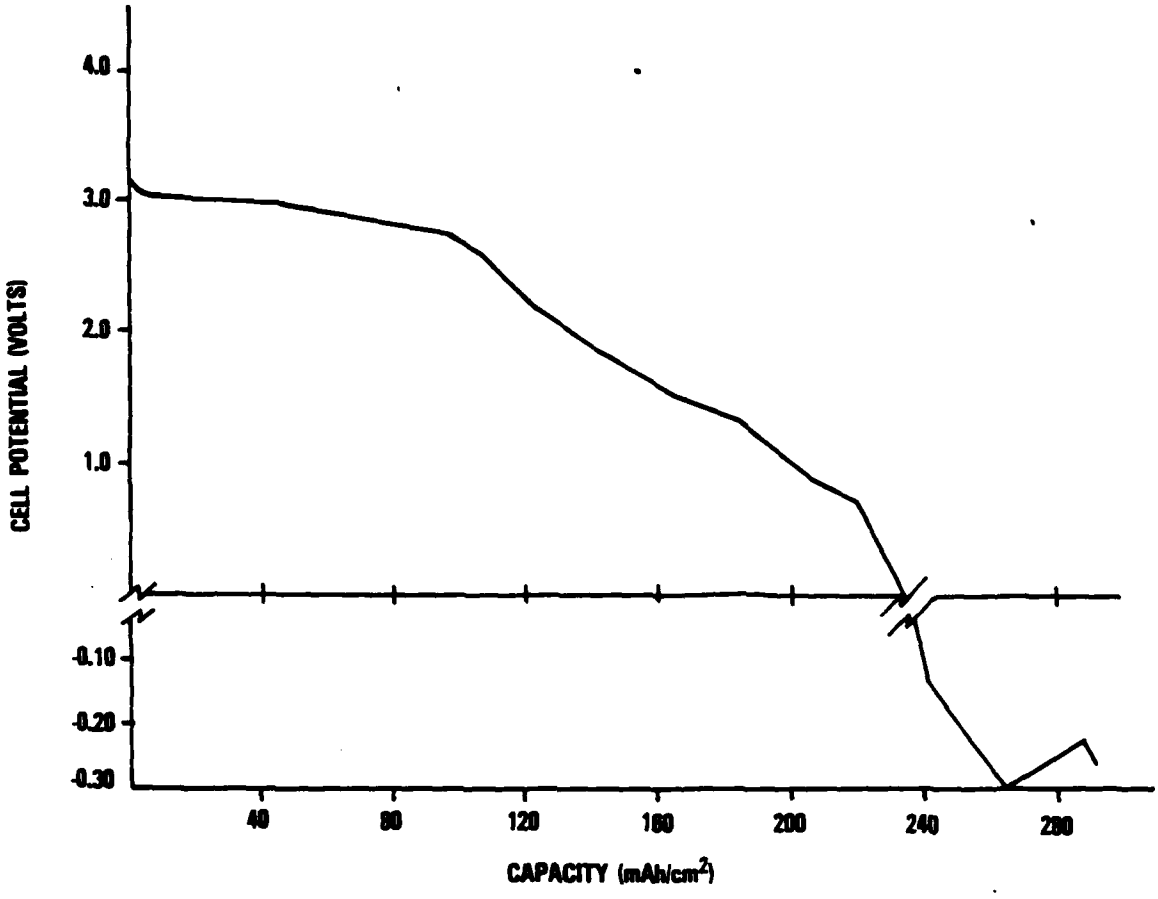

The cell was discharged at 0.50 mA/cm^2 constant current, then overdischarged at 1.5 mA/cm^2.

Figure 29. Behavior of a Cathode Limited $Li/SOCl_2$ Cell During Discharge and Overdischarge at 1.5 mA/cm^2 at -40°C

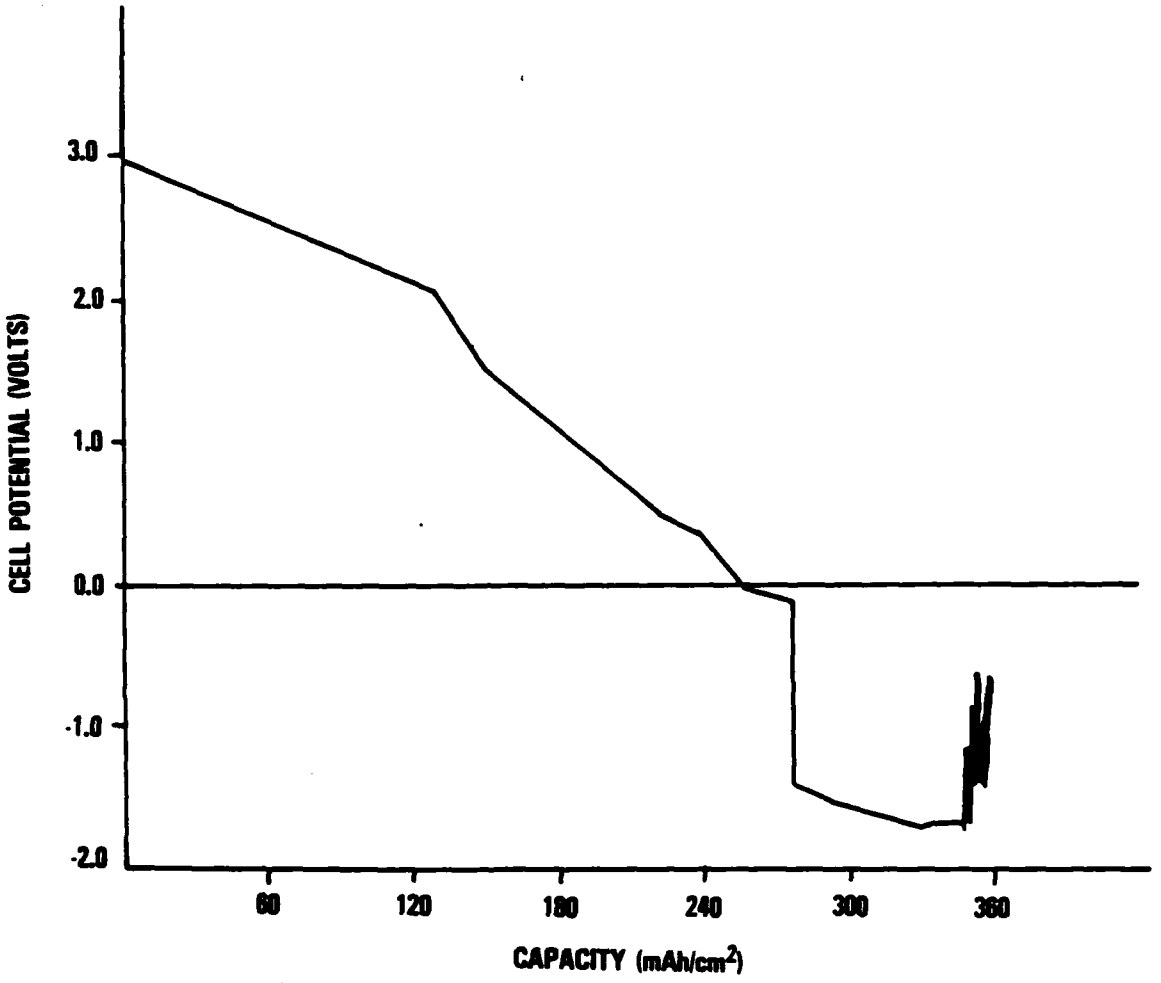

The cell was discharged at 1.0 mA/cm^2, then overdischarged at 1.0 mA/cm^2 for 24.2 mAh/cm^2. It was next overdischarged an additional 81.3 mAh/cm^2 at 10 mA/cm^2.

Figure 30. Behavior of a Cathode Limited Li/$SOCl_2$ Cell During Discharge and Overdischarge at 10 mA/cm^2 at -40°C

conductivity of the electrolyte at -40°C and the large IR drop due to the wide spacing of the electrode (i.e., 13 mm) it was not possible to discharge the cell much above 1.0 mA/cm^2 without excessive polarization. However, once the cell was overdischarged 24.2 mAh/cm^2 at 1.0 mA/cm^2, the current was increased to 10 mA/cm^2 because a sufficient amount of Li had been deposited on the cathode to permit overdischarge at 10 mA/cm^2 without excessive polarization.

The fluctuations in potential observed from 348 to 358 mAh/cm^2, shown in Figure 30, are characteristic of dendrite shorting. Due to the persistence of the intermittent shorting, overdischarge was voluntarily terminated when the total capacity reached 358 mAh/cm^2). Based on the nominal capacity of the cathode at 2 mA/cm^2 at 25°C (i.e., 372 mAh/cm^2, the cathode was 28.5 percent overdischarged. However, since dendrite shorts occurred,the actual overdischarge was somewhat less. The capacity achieved at 1 mA/cm^2 to reversal was 253 mAh/cm^2, thus, the cathode was, in principle, only 67 percent depleated.

At the end of overdischarge, the cell was immediately transferred from the refrigerated chamber to the dry room for 24 hours before being drained of electrolyte. During this period, 21 microphotographs were taken of the Li dendrites at magnifications of 3.8X and 19X. Twelve of the microphotographs were taken from six to 43 minutes after the end of overdischarge and the remainder were taken after 1.8, 3.5, 19, and 24 hours on OCV. No noticeable change in the Li dendrite morphology was observed during the first hour as the cell warmed up from -40° to 25°C, or during the first 3.5 hours on OCV. However, it is estimated that approximately 95 percent of the dendrite mass became detached from the cathode and disintegrated during the period from 3.5 to 19 hours. No further changes in the dendrites remaining on the cathode were observed from 19 to 24 hours. It was also observed that a large quantity of dendrites which had become detached and which were floating on the surface of the electrolyte at the end of overdischarge had dissolved during the period from 3.5 to 19 hours. After 19 hours very few detached dendrites were floating on the surface of the electrolyte and only a moderate amount of white powder, presumably LiCl, was observed on the bottom of the cell. Thus, it was concluded that the Li dendrites which had dissolved from 3.5 to 19 hours had reacted with intermediates from the reduction of $SOCl_2$ rather than having been anodically dissolved by being in electrical contact with the undepleted carbon cathode.

The 3.5-hour delay before the Li dendrites were corroded by $SOCl_2$ discharge intermediates could be the time required for the first intermediate complex to dissociate

into the second intermediate which may have reacted with the Li. The existence of a $SOCl_2$ reduction intermediate which builds up to a maximum concentration in approximately 16 hours after discharge at 25°C has been demonstrated by electroanalytical techniques referred to earlier. In commercial optimized Li/$SOCl_2$ cells, which contain a much higher electrode surface to electrolyte volume than the flooded cells used for the present overdischarge studies, it would be expected that the first intermediate concentration would be much higher shortly after overdischarge and the buildup of the second intermediate would occur much sooner. This could lead to rapid chemical attack of the Li dendrites as soon as the cell, discharged a -40°, was allowed to warm up to 25°C. Such a rapid attack could lead to thermal runaway and unexpected explosions such as those occasionally reported when cells overdischarged at <-30°C are warmed to room temperature.

The X-ray diffraction peaks obtained for the carbon sample from the cathode discharged at -40°C, 10 mA/cm^2 are listed in Table 10. The diffraction pattern shows the peaks only for LiCl and not for the rhombic sulfur as found earlier for cells discharged at 25°C, mA/cm^2 and -40°C, 1.5 mA/cm^2.

The absence of the peaks for rhombic sulfur in the X-ray pattern may be due to the higher rate of discharge allowing less time for the $SOCl_2$ discharge intermediate to decompose. This reaction as well as other factors were discussed previously.

TABLE 10
DEBYE-SCHERRER X-RAY DIFFRACTION ANALYSIS OF CARBON FROM CATHODE LIMITED CELLS*

Discharged at -40°C at 10 mA/cm^2			Discharged at 40°C, 2 mA/cm^2		
d(A)	2θ	I/Io	d(A)	2θ	I/Io
2.97	30.06	100	2.95	30.26	90
2.57	34.88	90	2.56	35.02	90
1.818	50.12	60	1.81	50.36	50
1.550	59.58	50	1.55	59.60	30
1.485	62.48	40	1.48	62.72	10
1.285	73.64	30	1.172	87.20	10
1.180	81.50	30	1.145	87.44	10
1.150	87.38	30			
1.050	94.36	30			

*All diffraction results were obtained using CuKα radiation with a Ni filter.

Examination of the surface of the cathode at 40, 100, 300, and 1000X magnification using a scanning electron microscope (SEM) did not reveal the Li filaments seen earlier. However, stubs with a diameter of $4 \cdot 10^{-3}$mm, the same diameter as the Li filaments,

were observed as well as larger plates with a diameter of 10-15 10^{-3}mm. Since the cell was stored at room temperature for 24 hours before being drained of electrolyte, during which time 9[illegible]ercent of the dendrite mass became detached, the dendrite stubs seen by SEM fit in well with the cells' history. The stubs are probably the points where the Li filaments were corroded and the bulk of the mass became detached from the surface of the carbon electrode. The chemical reaction causing corrosion of the Li dendrites during the 24 hours of 25°C storage were discussed earlier.

Cross sections of the cathode from the carbon limited cell discharged at 10 mA/cm^2, -40°C were examined at 40, 300, and 1000X magnification using the SEM. No signs of electrodeposited Li in the interior of the cathode were observed. A total of seven SEM photographs were taken and are on file.

5.2.3 Overdischarge of Cathode Limited Cells at 40°C

Two cathode limited cells were overdischarged at 40°C, one at 2 mA/cm^2 and the other at 20 mA/cm^2. The cell discharged at 2 mA/cm^2, 40°C contained 1.490 g Li and 0.760 g carbon which would give theoretical capacities of 5.75 and 2.91 Ah (at 2 mA/cm^2). On overdischarge, dendrites were deposited in an unusually uniform manner over the surface of the cathode rather than just at a few points along the bottom or near the lead, as seen in a majority of the previous tests. The cell potentials during discharge are shown in Figure 31. The discharge capacity to 0.0V was 300 mAh/cm^2 and 364 mAh/cm^2 at the end of overdischarge when the current was voluntarily terminated and microphotographs taken of the dendrites.

Five high-quality microphotographs (3.8X magnification) were taken of the Li dendrites which show somewhat less resolution than earlier photographs because the electrolyte was slightly opaque due to suspended LiCl. The electrolyte was also an unusual orange-brown color and it is possible that at 40°C a greater amount of sulfur may dissolve which somehow assists in suspending LiCl particles which flake off the anode. The dendrites were similar to those observed at 2 mA/cm^2, 25°C and discussed earlier. However, SEM examination of Li dendrites deposited during overdischarge on the carbon electrode at 40° reveals a much denser structure, as shown in Figure 32, than observed at 25°, as illustrated in Figures 20 and 21. A total of 15 SEM photos were taken of the Li dendrites at several points on the cathode surface at magnifications ranging from 45X to 3000X. As shown in Figure 33, it was observed that the Li dendrite tips from the 40°C, 2 mA/cm^2 cell had three or more growing crystals at the tips compared to a single

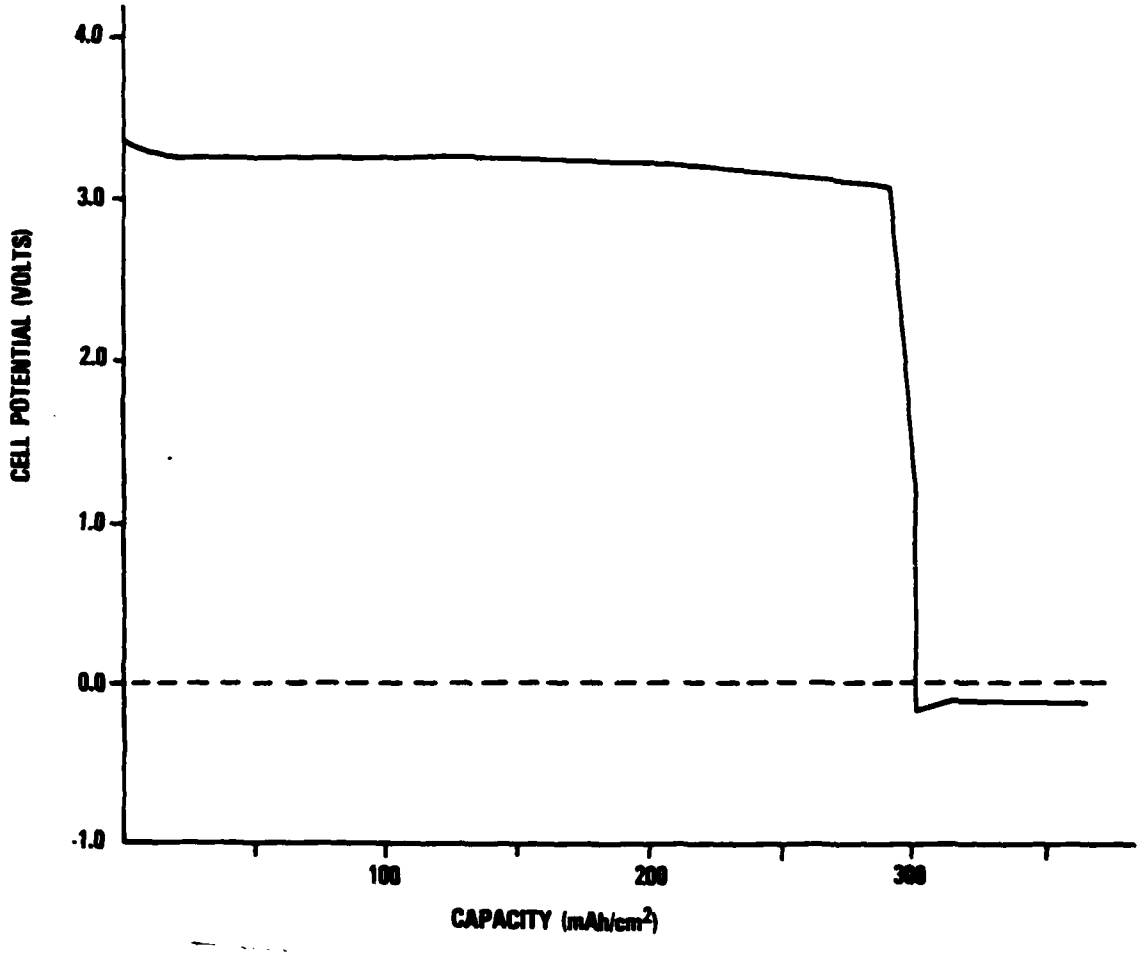

Figure 31. Behavior of a Cathode Limited Cell During Discharge and Overdischarge at 40°C, 2.0 mA/cm²

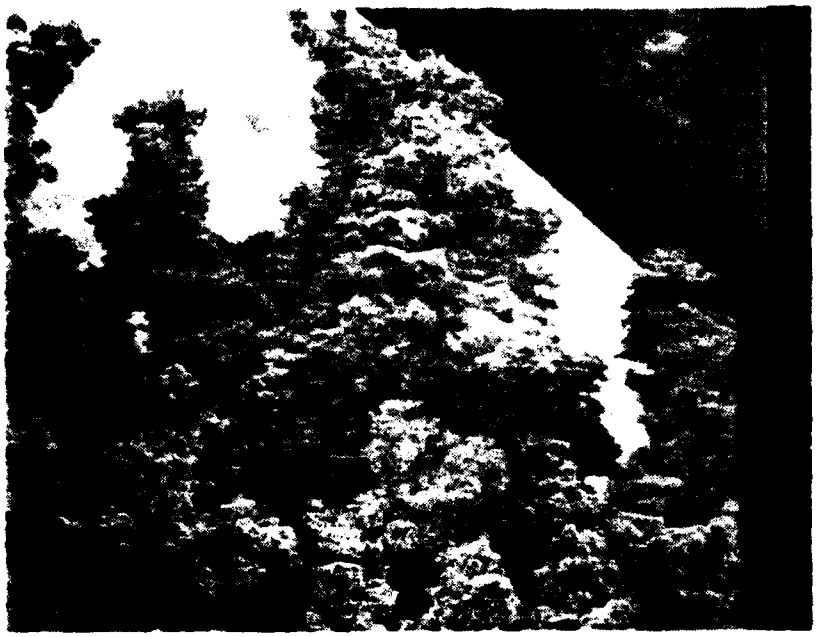

Figure 32. SEM Photograph of Lithium Dendrites on Surface of Cathode Overdischarged at 40°C, 2mA/cm^2 (45X Magnification, View at 45°)

Figure 33. SEM Photograph of Lithium Dendrite Tips of Cathode Shown Above (3000X Magnification)

growing crystal filament about 1/5 of size observed at 25°C. These observations indicate to us that it may be possible to change the cell chemistry or design so that the Li dendrites produced on overdischarge are denser and capable of carrying more current on overdischarge. Such thicker Li dendrites would probably be less likely to melt and initiate an explosion when a short circuit is produced by growth of the dendrites across to the anode.

Five SEM photos of a cross section of the carbon cathode from the cathode limited cell overdischarged at 40°C, 2 mA/cm^2 were taken at magnifications of 45X, 100X, 300X, 1000X, and 3000X. No signs of metallic Li deposition in the interior of the carbon electrode were observed.

The X-ray diffraction peaks obtained for the carbon sample from the cathode discharged at 40°C, 2 mA/cm^2 are listed in Table 10. The diffraction pattern shows the peaks only for LiCl and not for rhombic sulfur as found for the cell overdischarged at 2.0 mA/cm^2 at 25°C. The higher solubility of sulfur at 40°C may account for its absence in the X-ray pattern.

The second cathode limited cell at 40°C was overdischarged at 20 mA/cm^2, contained 0.764 g of carbon, and was of the same design as used earlier. The cell potentials during discharge and overdischarge at 20 mA/cm^2 are shown in Figure 34. On discharge the cell delivered 77.36 mAh/cm^2 to reversal, then it was overdischarged 89.3 mAh/cm^2 until the test was voluntarily terminated. The lithium dendrites which formed on overdischarge were distributed very uniformly over the surface, similar to the cell overdischarged at 2 mA/cm^2 at 40°C discussed earlier. No sudden fluctuation in cell potential indicative of dendrite shorting were recorded during overdischarge even though it appeared that the Li dendrites had grown across the ~6 mm interelectrode gap to touch the Li anode.

A total of nine SEM photographs were taken of the Li dendrites at several points on the cathode surface at magnifications ranging from 40X to 3000X. Figure 35 illustrates the strange combination of morphologies that were observed for the Li deposited at 20 mA/cm^2, 40°C. The tips of the dendrites showed three or more growing crystal surfaces but the sides of the dendrite nodules showed Li filaments similar to those observed at 25°C at 2 mA/cm^2. Figure 36 shows a portion of the tip of the dendrite nodule shown in Figure 35 with the magnification increased from 300X to 3000X. The three or more Li crystals at the tip of the Li dendrites are clearly defined. Although a comparison of Figures 33 and 36 suggests a larger number of Li crystals at the tips of

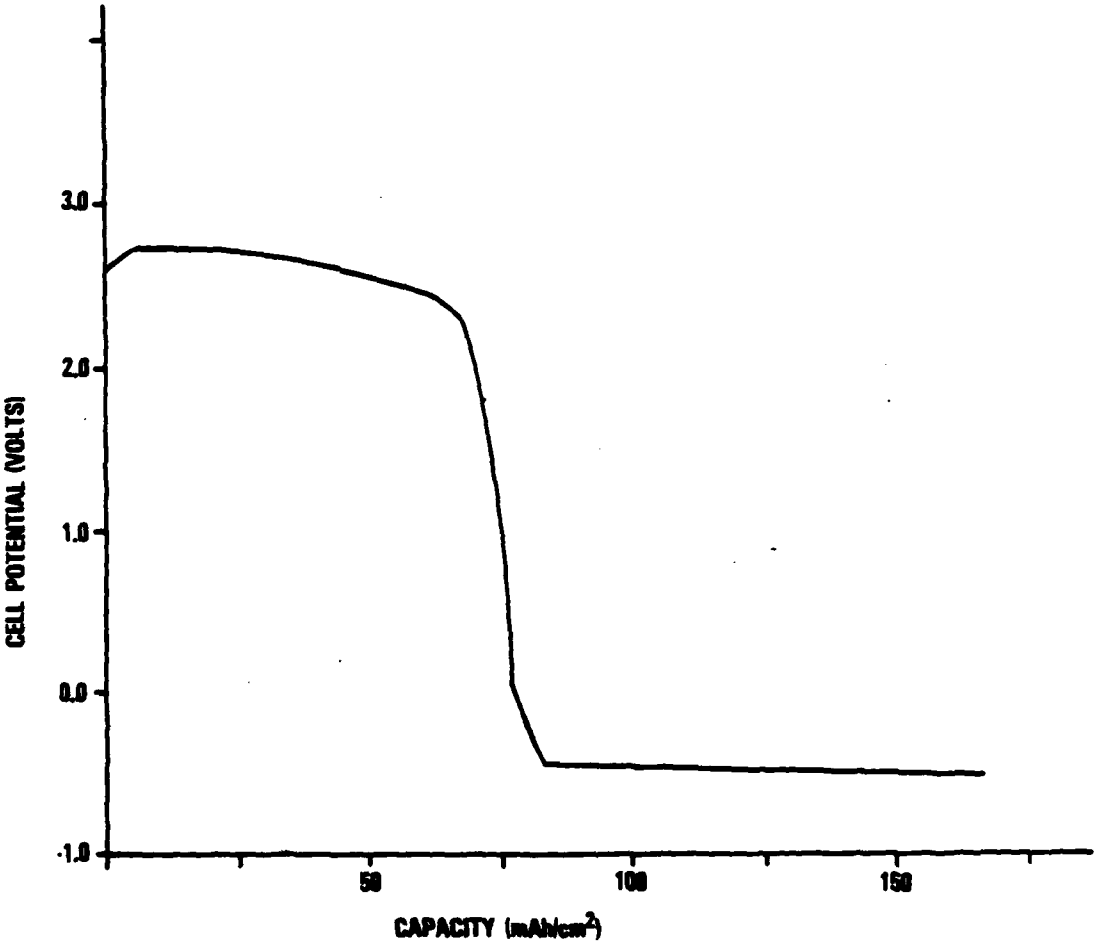

Figure 34. Behavior of a Cathode Limited Li/$SOCl_2$ Cell During Discharge and Overdischarge at 20 mA/cm^2 at 40°C

Figure 35. SEM Photograph of Lithium Dendrites on Surface of Cathode Overdischarged at 40°C, 20 mA/c¬¹² (300X Magnification, View at 45°)

Figure 36. SEM Photograph of Lithium Dendrite Tips of Cathode Shown Above (3000X Magnification)

the dendrites deposited at 2 mA/cm^2, an examination of all 24 of the SEM photographs indicates that the morphology of the dendrite tips is similar at both 2 and 20 mA/cm^2 at 40°C.

Seven SEM photos of a cross section of the carbon cathode from the cathode limited cell overdischarged at 40°C, 20 mA/cm^2 were taken at magnifications of 45X, 100X, 300X, 1000X, and 3000X. No signs of metallic Li deposition in the interior of the cathode were observed at 100X or below but at higher magnification pieces of Li filaments similar to those shown in Figure 22 were observed. It is thought that the Li filaments were not deposited in the interior of the cathode but were accidentally introduced during the preparation of the samples for SEM examination.

The X-ray diffraction peaks obtained for the carbon sample from the cathode discharged at 20 mA/cm^2, 40°C are listed in Table 11. The results and interpretation is the same as given earlier for the X-ray results for the cathode overdischarged at 2 mA/cm^2, 40°C. There is one slight difference however, the weak line at 1.278 A which it is thought is due to the 1.283 line of Li_2O_2. The appearance of Li_2O_2 was observed in other cells and may be due to the oxidation of the Li dendrites during cell disassembly and then contamination during sampling.

5.2.4 Overdischarge of Anode Limited Cells at 25°C

Two anode limited cells were overdischarged at 25°C, one at 2 mA/cm^2 and the other at 20 mA/cm^2. The theoretical capacity of the anode and cathode of the cell overdischarged at 2 mA/cm^2 were 1.07 and 3.05 Ahr, respectively. The behavior or the cell potential during discharge at 2.0 mA/cm^2 and overdischarge at 0.59 mA/cm^2 is shown in Figure 37.

The cell was overdischarged until the total capacity reached 3.384 Ah (i.e., 376 mAh/cm^2) without any increase in polarization above that recorded during the period following reversal. It was, therefore, concluded that the cathode was not passivated as usual at 3.05 Ah because the LiCl discharge product was dissolved by $AlCl_3$ produced at the anode during overdischarge. The electrode reaction at the Ni screen of the anode during overdischarge after all the Li has been consumed is most likely oxidation of SO_2; $2\ AlCl_4^- + 2\ SO_2 \rightarrow SO_3 + SOCl_2 + 2\ AlCl_3 + 2e$ as discussed above.

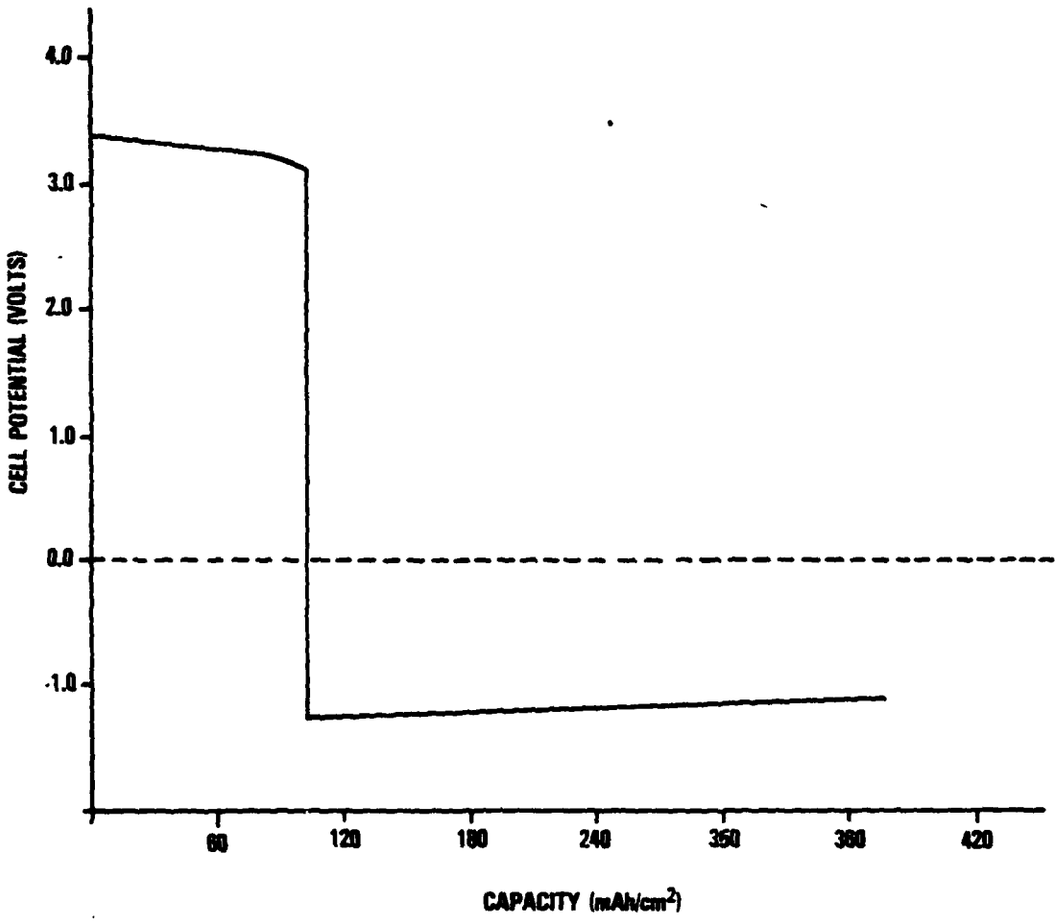

The cell was discharged at 2.0 mA/cm^2 constant current with reversal at 103 mAh/cm^2. It was then overdischarged at 0.59 mA/cm^2.

Figure 37. Behavior of an Anode Limited Li/$SOCl_2$ Cell During Discharge and Overdischarge at 2.0 mA/cm^2, 25°C

No signs of a blue or green coloration of the electrolyte were observed which indicates that the nickel screen was essentially inert to anodic dissolution. The design of the anode limited cell used in the present work would favor Li deposition on overdischarge, if Li deposition was possible, because of the large excess of Li ions in the large volume of electrolyte. With 168 ml of 1.8M $LiAlCl_4/SOCl_2$, the electrolyte contained enough Li to permit the cathode to operate 8.14 Ah, considerably over the 3.05 Ah theoretical capacity of the cathode.

The results suggest that at low rates, $SOCl_2$ consumption, leading to electrolyte starvation rather than Li deposition, may be the major safety hazard involved in the overdischarge of anode limited cells. Electrolyte starvation could possibly lead to explosions caused by local heating as the electrolyte level dropped and more current was forced through increasingly smaller electrode areas.

The X-ray diffraction peaks obtained for carbon from the anode limited cell are listed in Table 11. The diffraction pattern shows the peaks only for LiCl and not for rhombic sulfur, as found earlier for cathode limited cells discharged at 25°C, 2 mA/cm^2. The cause for the absence of the peaks for rhombic sulfur is not known but it may be related to the partially discharged state of the cathode providing enough porosity for the sulfur to dissolve out of the cathode by diffusion during the 14 days required for the overdischarge.

Cross sections of the cathode from the anode limited cell discharged at 2 mA/cm^2, 25°C were examined at 40X, 100X, 300X, and 1000X magnification using the SEM. No

TABLE 11
DEBYE-SCHERRER X-RAY DIFFRACTION ANALYSIS OF CARBON FROM CATHODE AND ANODE LIMITED CELLS*

Anode Limited Cell Discharged at 25°C at 2 mA/cm^2			Cathode Limited Cell Discharged at 40°C, 20 mA/cm^2		
d(A)	2θ	I/Io	d(A)	2θ	I/Io
2.96	30.16	100	2.95	30.26	100
2.57	34.88	100	2.55	35.16	100
1.81	50.36	90	1.81	50.36	90
1.545	59.80	60	1.545	59.80	50
1.482	62.62	50	1.480	62.72	30
1.283	73.78	40	1.278	74.12	10
1.178	81.66	50	1.173	87.16	30
1.148	84.28	50	1.145	87.44	30
1.047	94.72	50			

*All diffraction results were obtained using CuKα radiation with a Ni filter.

signs of electrodeposited Li were observed in the interior of the cathode. A total of seven SEM photographs were taken and are on file.

The second anode limited cell at 25°C which was overdischarged at 20 mA/cm^2 utilized two Li anodes and a cathode with theoretical capacities of 1.091 and 2.385 Ah, respectively. The cathode capacity was calculated based on a carbon loading of 0.7389 g and the capacity of a similar cathode discharged at 2 mA/cm^2. The behavior of the cell potential during discharge and overdischarge at 20 mA/cm^2 is shown in Figure 38. The cell went into reversal after delivering 0.54 Ahr; therefore, the anode efficiency at 20 mA/cm^2 was 49.4 percent. Since, based on earlier results, 0.88 Ahr was expected from the cathode at 20 mA/cm^2, the cell was clearly anode limited. The cell became both anode and cathode limited when the cell potential reached -5.8V at a capacity of approximately 0.89 Ah. Lithium dendrites were first noticed on the surface of the carbon cathode after 2.48 hours of discharge when the capacity had reached 0.892 Ahr. As the overdischarge was continued, the Li dendrites on the surface of the carbon continued to grow until they extended about 1.5 mm into the electrolyte, as shown in Figure 39.

Lithium deposition would not be expected in anode limited cells because the $AlCl_3$ and SO_3 produced by oxidation of SO_2 at the Ni anode during overdischarge would prevent the cathode from becoming passivated by dissolving the LiCl to form $LiAlCl_4$. Furthermore, any Li dendrites formed would be rapidly corroded by both the SO_3 and the $AlCl_3$. Lithium dendrites, however, were deposited on the cathode during overdischarge at 20 mA/cm^2, but not at 0.59 mA/cm^2, probably because the $AlCl_3$ and SO_3 couldn't diffuse across the 6 mm interelectrode space fast enough at the higher rate.

If Li deposition is only possible in anode limited cells because of a diffusional lag effect, then it would be expected that the dendrites would be rapidly corroded once the high rate overdischarge was terminated. This possibility was investigated and it was found that significant corrosion occurred during the first 16 minutes on open circuit as is evident by comparing Figures 39 and 40.

As soon as the cell was placed on open circuit, small thin filaments of Li could be seen under the stereomicroscope breaking off the dendrite mass and floating to the surface of the electrolyte. This type of corrosion gradually subsided after about ten

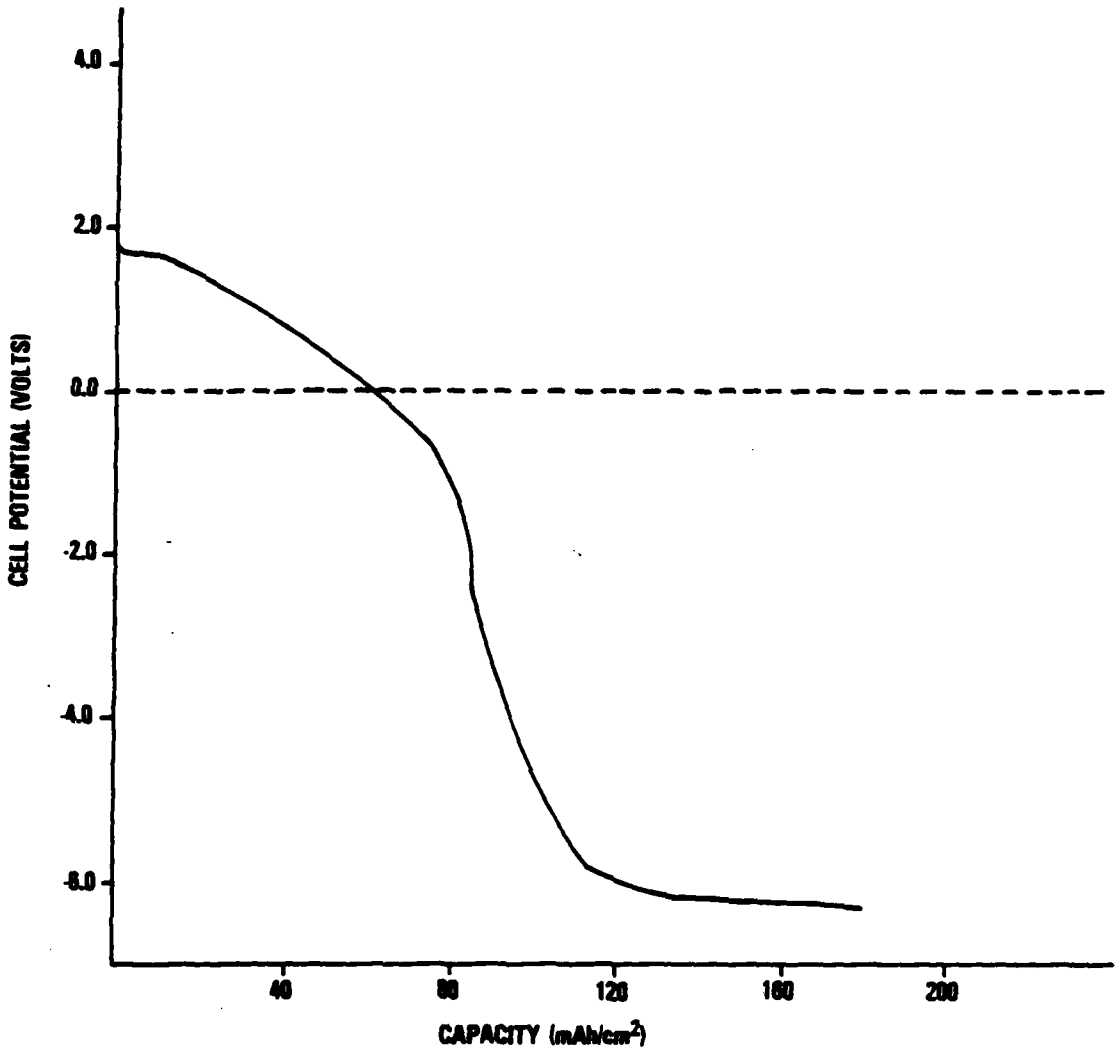

The capacity was calculated on the basis of a cathode area of 9 cm^2

Figure 38. Behavior or an Anode Limited $Li/SOCl_2$ Cell During Discharge and Overdischarge at 20 mA/cm^2 at 25°C

Figure 39. Lithium Dendrites on Overdischarged Cathode From an Anode Limited Cell (15.2X Magnification), After 2 Sec. on Open Circuit; Cell Overdischarged 128.0 mAh/cm^2 at 20.0 mA/cm^2, 25°C

Figure 40. Lithium Dendrites on Overdischarged Cathode From the Anode Limited Cell Shown Above (15.2X Magnification) but After 16 Minutes on Open Circuit

minutes resulting in the removal of most of the sharp projections and nodules, and a general smoothing of the dendrite mass as shown in Figure 40. After 15 minutes on open circuit, the dendrites had begun to lose their metallic luster and the rate of corrosion appeared to be greatly reduced. However, after overnight stand on open circuit (i.e., 16.5 hr.), all the Li dendrites were consumed by corrosion. Thus, $AlCl_3$ and SO_3 produced at the Ni anode screen on overdischarge, most likely reacted with the Li dendrites, but the corrosion rate was much slower than initially expected.

Overdischarge of the anode limited cell was resumed after 22 hours on open circuit to discover if Li could be deposited again. During this second 1.88-hour period of overdischarge at 20 mA/cm^2, the cell potential changed from -4.14V at the start to -18.2V, but Li deposition was not observed. The overdischarge was terminated when the potential reached -18.20V because the cell was consuming about 6.5 watts and had heated to about 50°C. Evidently the thickened LiCl film provides too great an overpotential for lithium deposition.

The results of the present experiments with anode limited cells carried out with an interelectrode spacing of 6 mm should be interpreted with caution when applied to the design of commercial cells with interelectrode spacings of 1 mm or less. At 1 mm or closer electrode spacings, Li dendrites may not form on overdischarge at 20 mA/cm^2, 25°C because the $AlCl_3$ and SO_3 formed on the bare Ni anode screen have a very short diffusion path to the cathode.

The electrolyte was drained from the cell discharged at 20 mA/cm^2 within 1 minute after termination of the second overdischarge and the cathode was immediately evacuated in a vacuum desiccator. After two days under vacuum ($\sim 100\mu$) a sample of the carbon was prepared for X-ray diffraction analysis as described earlier. The X-ray diffraction peaks that were obtained are listed in Table 12. The diffraction pattern shows peaks for LiCl, Li_2O_2, and a few weak peaks for rhombic sulfur. The anode limited cell discharge at 2 mA/cm^2 showed peaks only for LiCl and it is not known why increasing the rate to 20 mA/cm^2 should increase the content of rhombic sulfur in the cathode. It is possible that at the higher rate, the cathode was sealed with a skin of LiCl preventing the sulfur from dissolving and diffusing out in the shorter discharge period. The detection of Li_2O_2 in the cathode indicates that the Li dendrites were probably not all converted into LiCl, but a substantial amount of metallic Li remained on the surface or inside the carbon cathode.

TABLE 12
DEBYE—SCHERRER X-RAY DIFFRACTION ANALYSIS OF CARBON FROM AN ANODE LIMITED CELL OVERDISCHARGED AT 20 mA/cm^2, 25°C*

d(A)	2θ	I/Io
3.80	23.39	30
3.43	25.95	10
2.94	30.38	9
2.72	32.90	100
2.57	34.86	90
2.45	36.64	5
2.22	40.60	20
2.03	44.60	5
1.91	47.56	35
1.86	48.92	20
1.82	50.07	50
1.71	53.54	7
1.56	59.16	50
1.54	60.02	40
1.475	62.96	20
1.352	68.30	20
1.278	74.12	10
1.21	79.07	10
1.173	82.09	20
1.145	84.55	30
1.044	95.09	20
1.022	97.79	10

*The diffraction results were obtained using CuKα radiation with a Ni filter.

Six SEM photos of a cross section of the carbon cathode from the anode limited cell were taken at magnification of 45X, 300X, 600X, and 3000X. At the higher magnifications, a large number of cubic crystals, most likely LiCl, about $3 \cdot 10^{-3}$ mm in size, were observed, but there were no signs of metallic Li deposits.

5.2.5 Electrochemical Kinetics of Lithium Dendrite Formation

From the review of the electrochemical kinetics of metal deposition in aqueous solutions by Vetter[31], it appears that the theory developed by Price, Vermiyea, and Webb[18] would be useful to understand Li dendrite formation in Li/$SOCl_2$ cells. According to Vermilyea, metal may be deposited in the form of long fine threads, so-called whiskers, when some substance is absorbed at different concentrations on the various surfaces of the crystallite of the first growing nucleus. It is assumed that the absorbed substance is incorporated into the deposited metal.

In the case of Li deposition in $SOCl_2$, the current density at the growing crystal surface would have to be so large that the LiCl would be incorporated more rapidly into the Li metal crystal than $SOCl_2$ can react with Li to form LiCl. The various surfaces of the Li crystals will have different reaction rates with $SOCl_2$ to form LiCl, with eventually only one surface continuing to grow. If this is the front surface, a whisker is formed which continues to grow at this front surface, while the growth at the side surfaces has stopped.

This account of Vermilyea's explanation for whisker growth is only a very brief simplified account of the theory which was published with a convincing mathematical description of the reaction kinetics and supported by experimental data. Of particular interest to improving the safety of $Li/SOCl_2$ cells during overdischarge is the finding that the specific conductivity of whiskers of Ag grown in aqueous solutions are two or three smaller than the value for pure Ag because of the high concentration of incorporated impurities.

Vermilyea's explanation of the kinetics of whisker growth implies that substances could be added to the $SOCl_2$ electrolyte which would change the mechanism of crystal growth. In principle, the additives would be absorbed in such a way as to increase the amount of LiCl in the Li dendrite deposits. Or alternatively a different class of additives could be used to make the dendrites thicker with less included LiCl. Such dendrites would probably be much less hazardous because they could carry more current without melting when the interelectrode gap was bridged by the dendrite during overdischarge or charging. At the present time there is not sufficient data to determine whether dendrites with more or less LiCl are the most desirable to make a safer cell.

6.0 CONCLUSIONS

No hazardous reactions were encountered associated with discharge or overdischarge at 1mA/cm^2 and room temperature. Intermediate species on discharge and cathode limited overdischarge do not develop substantial concentrations. Addition complexes of $LiAlCl_4$, SO_2, and $SOCl_2$ along with elemental sulfur account for most of the spectrascopic data. Sulfur exists in part as a long lived stable free radical. A second radical is detected with a lifetime on the order of days. SO_3 is suspected as a product of intermediate decomposition.

Anode limited overdischarge produces some SO_3 and probably S_2Cl_2 through oxidation of SO_2. Reaction of oxidation products with lithium dendrites prevents buildup of intermediates and total consumption of SO_2 or $SOCl_2$. No evidence was found for Cl_2, SO_2Cl_2, Cl_2O, or SO^{2+} as suggested in earlier studies, though two new radicals appear on anode limited overdischarge.

Lithium dendrites grow on the surface of the cathode in cathode limited overdischarge at all temperatures and current densities investigated. In anode limited overdischarged cells, dendrites can be formed at elevated current densities and presumably at low temperature. At 1mA/cm^2 and room temperature, dendrites were consumed evenly by oxidation products of anode limited overdischarge.

No evidence was found in either X-ray diffraction patterns or electron micrographs for lithium-graphite intercalation compounds. No evidence was found for dendrite growth or movement due to Ostwald ripening. Dendrites decompose quickly due to self-discharge on the cathode and reaction with various oxidants. Apparently the dendrites are segmented by small areas of LiCl. This helps moderate the dendrite decomposition and prevents sufficient conductivity to sustain interelectrode shorts.

One potential hazard implicated is the situation where strong oxidants such as SO_3 are produced on overdischarge at low temperature but because of sluggish diffusion rates and reaction kinetics, no reaction occurs with lithium until the cell is warmed. A related hazard may occur in cells which go into overdischarge, as those of Abraham et al, because of detachment of lithium from the current collector. Under these circumstances, the oxidation products have only a short distance to diffuse over to a fresh lithium surface. The last hazard identified as a possibility on overdischarge may occur when a cell becomes electrolyte limited. Here the ohmic heating can become substantial and pressure may build up from the breakdown of $LiAlCl_4 \cdot 3SO_2$.

Further work in these areas is desirable, especially in simulating the proposed hazard scenarios.

REFERENCES

1. K. M. Abraham, R. M. Mank and G. L. Holleck, ERADCOM, DELET-TR-0564F Final Report for Contract No. DAABOF-78-C-0564m 'Investigations of the Safety of $Li/SOCl_2$ Batteries'.
2. K. M. Abraham and R. M. Mank, J. Electrochem. Soc. 127, 2091 (1980). 'Some Chemistry in the $Li/SOCl_2$ cell'.
3. D. J. Salmon, M. E. Adamczyk, L. L. Studer, L. L. Abels and J. C. Hall, Abstract No. 62, Electrochemical Society Meeting, 1980, Hollywood, Fla., 'Spectroscopic Studies of the Hazards of $Li/SOCl_2$ Batteries During Cell Reversal.
4. TRW Document, Qualification and Characterization Testing of Minuteman Lithium Power Source (BMO Transmittal Serial No. 3054-KH-Kh 8900-WPF).
5. F. Goebel, R. C. McDonald, and N. Marincic, 'Proceedings on the 29th Power Sources Conference,' Atlantic City, New Jersey, June, 1978, The Electrochemical Society, Inc. P168 (1981).
6. Report No. 0001-141A2-3D, 'Lithium Power Source Draft Final Engineering Report', Contract No. F04704-78-C-0001, March 1980. BMO, Page AJ-1 Appendix AJ.
7. Report No. AF WAL-TR-80-2121, F. Goebel, R. McDonald and G. Younger, 'Lithium Inorganic Electrolyte Battery', Contract No. 0001 Wright Patterson Air Force Base, p. 55.
8. F. Goebel, R. McDonald, and N. Marincic, Proc. of the 15th I.E.C.E.C. Meeting, Seattle, Wash., August 1980, 'Performance Characteristics of the Minuteman Lithium Power Source'.
9. W. P. Kilroy and S. D. James, J. Electrochemical Soc. 128, 93A (1981). 'Promotion by Carbon of the Reactivity of Lithium with $SOCl_2$ and SO_2 - Effect on Lithium Battery Safety'.
10. C. Schlaikjer, F. Goebel and N. Marincic, J. Electrochemical Soc., 126, 513, (1979).
11. P. Barbier, Y. Beder, J. Corset, M. C. Dhamelincourt, F. Wallart, Int. Meeting on Lithium Batteries, Rome, April 27-29, 1982.
12. R. C. McDonald, J. Electrochem. Soc., 129, 2453 (1982).
13. D. A. Long and R. T. Bailey, Trans. Farad. Soc., 59, 594 (1963).
14. G. Nickless, (ed.) 'Inorganic Sulfur Chemistry', Elsevier, New York (1968).
15. W. K. Istone and R. J. Brodd, J. Electrochem. Soc., 129, 1855 (1982).

16. S. Bhagavantam, Indian J. Chem 8, 35 (1930).
17. R. J. Gillespie and E. A. Robinson, Can. J. Chem. 39, 2190 (1961).
18. P. B. Price, D. A. Vermilyea and M. B. Webb, Acta. Met. 6524 (1958).
19. D. L. Chua, S. L. Deshpande and H. V. Vankatasetty, 'Battery Design and Optimization', S. Gross ed., Electrochem. Soc. Fall Meeting, Pittsburgh, 1978.
20. D. J. Salmon and G. R. Ramsay, Proc. of the Symp. on Power Sources for Biomedical Applications, B. B. Owens and N. Margalit eds., 80-4, 1980.
21. D. J. Salmon, M. E. Adamczyk, L. L. Hendricks, L. L. Abels and J. C. Hall, Proceedings of the Symposium on Lithium Batteries, H. J. Vankatasetty, 81-4, p. 65 (1981).
22. G. Schwalbe, S. Schonherr and W. Windsch, Phys. Rev. Letters, 45, 356 (1977).
23. R. Hubin and Z. Gabelica, Thermochim. Acta, 20, 395 (1977).
24. B. Carter, A. Rodriquez, F. Tsay, S. Kim, R. Williams, M. Evans, L. Whitcanack, and H. Frank. Final Report on 'Safety Studies of Primary Lithium Batteries', J.P.L., Pasadena, CA 1982.
25. H. Low and R. Beandet, J. Amer. Chem. Soc., 98, 3849 (1976).
26. R. Hubin and Z. Gabelica, Thermochim Acta, 20, 395 (1977).
27. I. M. Kolthoff and Eggertsen, J. Am. Chem. Soc., 63, 1412 (1941).
28. W. Ostwald, Z. Physik, Chem. Leipzig, 34, 495 (1900).
29. S. Basu, C. Zeller, P. J. Flanders, C. D. Fuerst, W. D. Johnson, and J. E. Fischer, Materials Sci. Eng., 38, 275 (1979).
30. W. L. Bowden and A. N. Dey, J. Electrochem. Soc. 127, 1419 (1980).
31. K. J. Vetter, 'Electrochemical Kinetics', Academic Press, New York (1967).

DISTRIBUTION

	Copies
Defense Documentation Center Cameron Station Alexandria, VA 22314	12
Defense Nuclear Agency Attn: Library Washington, DC 20301	2
Institute for Defense Analyses R&E Support Division 400 Army-Navy Drive Arlington, VA 22202	1
Naval Material Command Attn: Code 08T223 Washington, DC 20360	1
Office of Naval Research Attn: G. Neece (Code ONR 472)	1
J. Smith	1
800 N. Quincy Street Arlington, VA 22217	
Naval Research Laboratory Attn: A. Simon (Code NRL 6130)	1
Code NRL 6100	1
4555 Overlook Avenue, S.W. Chemistry Division Washington, DC 20360	
Naval Postgraduate School Attn: Dr. William M. Tolles (Code 612)	1
Dr. Oscar Biblarz	1
Monterey, CA 93940	
Naval Air Systems Command Attn: Dr. H. Rosenwasser (Code NAVAIR 301C)	1
E. Nebus (Code NAVAIR 5332)	1
Washington, DC 20361	
U.S. Army Electronics Command Attn: A. J. Legath (Code DRSEL-TL-P)	1
E. Brooks (Code DRSEL-TL-PD)	1
G. DiMasi W. K. Behl Dr. Sol Gilman (Code DELET-PR)	1
Fort Monmouth, NJ 07703	
Callery Chemical Company Attn: Library Callery, PA 16024	1

	Copies
Naval Electronic Systems Command Attn: A. H. Sobel (Code PME 124-31)	1
Washington, DC 20360	
Naval Sea Systems Command Attn: F. Romano (Code 63R3)	1
E. Anderson	1
E. Daugherty (Code 06113)	1
J. Pastine (Code 06R)	1
Washington, DC 20362	
Strategic Systems Project Office Attn: K. N. Boley (Code NSP 2721)	1
M. Meserole (Code NSP 2722)	1
Department of the Navy Washington, DC 20360	
Naval Air Development Center Attn: J. Segrest (Code 6012)	1
R. Schwartz (Code 30412)	1
Warminster, PA 18974	
Naval Intelligence Support Center Attn: Dr. H. Ruskie (Code 362)	1
Washington, DC 20390	
Naval Ocean Systems Center Attn: Dr. S. Spazk (Code 6343)	1
San Diego, CA 95152	
U.S. Development and Readiness Command Attn: J. W. Crellin (Code DRCDE-L)	1
5001 Eisenhower Avenue Alexandria, VA 22333	
RAY-O-VAC Attn: R. Foster Udell	1
101 East Washington Avenue Madison, WI 53703	
Litton Data Systems Division	1
Attn: Frank Haluta, MS 64-61 8000 Woodley Avenue Van Nuys, CA 91409	
Lawrence Berkeley Laboratory Attn: F. McLamore	1
University of California Berkeley, CA 94720	

Rockwell International
Attn: Dr. Samuel J. Yosim 1
Atomics International Division
8900 DeSoto Avenue
Canoga Park, CA 91304

Stanford University
Attn: C. John Wen 1
Center for Materials Research
Room 249, McCullough Building
Stanford, CA 94305

EDO Corporation
Attn: E. P. DiGiannantonio 1
Government Products Division
2001 Jefferson Davis Highway
Arlington, VA 22202

Globe Union , Inc.
Attn: Dr. R. A. Rizzo 1
5757 N. Green Bay Avenue
Milwaukee, WI 53201

University of Missouri, Rolla
Attn: Dr. J. M. Marchello 1
210 Parker Hall
Rolla, MO 65401

RAI Research Corporation
Attn: Dr. Carl Perini 1
225 Marcus Boulevard
Hauppauge, NY 11787

Battery Engineering
Attn: Dr. N. Marincic 1
80 Oak Street
Newton, MA 02164

Honeywell Corporate Technology Center
Attn: H. V. Venkatasetty 1
Steven Schafer 1
10701 Lyndale Ave. So.
Bloomington, MN 55420

Honeywell, Inc.
Mat & Process Eng.
K. Y. Kim MN11-1812 1
600 2nd St., N.E.
Hopkins, MN 55343

The Aerospace Corporation
Attn: Harlan Bittner 1
P.O. Box 92957
Los Angeles, CA 90009

Honeywell Power Sources Center
Attn: Dr. D. L. Chua 1
N. Doddapeneni 1
104 Rock Road
Horsham, PA 19044

TRW Systems
Attn: I. J. Groce 1
G. L. Juvinal 1
Ed Moon, Rm. 2251, Bldg. 01 3
One Space Park
Redondo Beach, CA 90278

ALTUS Corporation
Attn: Dr. Adrian E. Zolla, Library 2
1610 Crane Court
San Jose, CA 95112

Capt. A. S. Alanis
BMO/ENBE
Norton AFB,
CA 92409 1

Norton AFB
Code AFISC/SES 1
CA 92409

PCI
Attn: Thomas Reddy 1
70 McQueston Parkway South
Mount Vernon, NY 10550

Dr. P. Bro
Hyde Park Estates 1
Santa Fe, NM 87501

Old Dominion University
Attn: R. L. Ake 1
Dept. of Chemical Sciences
Norfolk, VA 23508

U.S. Army Research Office
Attn: B. F. Spielvogel 1
P.O. Box 12211
Research Triangle Park, NC 27709

NASA Scientific and Technical Information Facility
Attn: Library 1
P.O. Box 33
College Park, MD 20740

National Bureau of Standards
Metallugy Division
Inorganic Materials Division
Washington, DC 20234 1

Battelle Memorial Institute
Defense Metals & Ceramics Information Center
505 King Avenue
Columbus, OH 43201 1

Bell Laboratories
Attn: Dr. J. J. Auborn 1
600 Mountain Avenue
Murray Hill, NJ 07974

Air Force Aero Propulsion
Laboratory
Attn: W. S. Bishop
(Code AFAPL/POE-1) 1
R. Marsh 1
(Code AFWAL-POOC-1) 1
Wright-Patterson AFB, OH 45433

Air Force Rocket Propulsion
Laboratory
Attn: LT. D. Ferguson
(Code MKPA) 1
Edwards Air Force Base, CA 93523

Headquarters, Air Force Special
Communications Center
Attn: Library 1
USAFSS
San Antonio, TX 78243

Office of Chief of Research
and Development
Department of the Army
Attn: Dr. S. J. Magram 1
Energy Conversion Branch
Room 410, Highland Building
Washington, DC 20315

Oak Ridge National Laboratory
Attn: K. Braunstein 1
Oak Ridge, TN 37830

Sandia Laboratories
Attn: Sam Levy (Mail Services
Section 3154-3) 1
P.O. Box 5800
Albuquerque, NM 87715

University of Tennesee
Attn: G. Mamantov 1
Department of Chemistry
Knoxville, TN 37916

University of Florida
Attn: R. D. Walker 11
Department of Chemical
Engineering
Gainesville, FL 32611

Attn: Library 1
Penn State University
University Park, PA 16802

Catalyst Research Corporation
Attn: G. Bowser 1
J. Joelson 1
A. Schneider 1
1421 Clarkview Road
Baltimore, MD 21209

Brookhaven National Laboratory
Attn: J. Sutherland 1
Building 815
Upton, NY 11973

California Institute of
Technology
Attn: Library 1
B. Carter 1
R. Somoano 1
H. Frank 1

Jet Propulsion Laboratory
4800 Oak Grove Drive
Pasadena, CA 91103

Argonne National Laboratory
Attn: Dr. E. C. Gay 1
9700 South Cass Avenue
Argonne, IL 60439

John Hopkins Applied Physics
Laboratory
Attn: Library 1
Howard County
Johns Hopkins Road
Laurel, MD 20810

Foote Mineral Company
Attn: H. R. Grady 1
Exton, PA 19341

Gould, Inc.
Attn: S. S. Nielsen 1
A. Attia 1
R. Putt 1
40 Gould Center
Rolling Meadows, IL 60008

GTE Laboratory
Attn: R. McDonald 1
R. Dampier 1
K. Kliendienst 1
W. Clark 1
520 Winter Street
Waltham, MA 02254

Hughes Aircraft Company
Attn: Dr. L. H. Fentnor 1
Aerospace Groups
Missile Systems Group Applied Research Laboratory
Tucson, AZ 85734

Saft Score, Inc.
Attn: L. A. Stein 1
200 Wight Avenue
Cockeysville, MD 21030

ESB Research Center
Attn: Library 1
19 W. College Avenue
Yardley, PA 19067

EIC Corporation
Attn: S. B. Brummer 1
K. M. Abraham 1
55 Chapel Street
Newton, MA 02158

Eagle-Picher Industries, Inc.
Attn: Robert L. Higgins 1
J. Dines 1
L. R. Erisman 1
Electronics Division
P.O. Box 47
Joplin, MO 64802

Union Carbide Battery Products Division
Attn: R. A. Powers 1
P.O. Box 6116
Cleveland, OH 44101

Wilson Greatbatch LTD.
Attn: Library 1
R. M. Carey 1
1000 Wehrle Drive
Clarence, NY 14030

Yardney Electric Corporation
Attn: Library 1
82 Mechanic Street
Pawcatuck, CT 02891

Naval Surface Weapons Center
Attn: W. P. Kilroy (Code R33) 12
New Hampshire Avenue
Silver Spring, MD 20910

Army Material and Mechanical Research Center
Attn: J. J. DeMarco 1
Watertown, MA 01272

USA Mobility Equipment R and D Command
Attn: J. Sullivan (Code DRXFB) 1
Code DRME-EC
Electromechanical Division
Fort Belvoir, VA 22060

Edgewood Arsenal
Attn: Library 1
Aberdeen Proving Ground
Aberdeen, MD 21010

Lockheed Missiles and Space Company, Inc.
Attn: Library 1
Lockheed Palo Alto Research Laboratory
3251 Hanover Street
Palo Alto, CA

Duracell Int., Inc.
Attn: B. McDonald 1
Battery Division
South Broadway
Tarrytown, NY 10591

Duracell Int., Inc.
Attn: W. Bowden 1
A. N. Dey 1
H. Taylor 1
Library 1
Laboratory for Physical Science
Burlington, MA 01803

Headquarters, Department of Transportation
Attn: R. Potter
(Code GEOE-3/61) 1
U.S. Coast Guard, Ocean Engineering Division
Washington, DC 20590

NASA Headquarters
Attn: Dr. J. H. Ambrus 1
Washington, DC 20546

NASA Goddard Space Flight Center
Attn: G. Halpert (Code 711) 1
Greenbelt, MD 20771

NASA Lewis Research Center
Attn: J. S. Fordyce
(Code MS 309-1) 1
M. Reid 1
2100 Brookpark Road
Cleveland, OH 44135

Naval Electronic Systems Command
Attn: T. Sliwa
(Code NAVELEX-01K) 1
Washington, DC 20360

Naval Weapons Center
Attn: Dr. E. Royce (Code 38) 1
Dr. A. Fletcher 1
China Lake, CA 93555

Naval Weapons Support Center
Attn: M. Robertson (Code 305) 1
D. Mains 1
Electrochemical Power Sources Division
Crane, IN 47522

Picatinny Arsenal
Attn: Dr. B. Werbel
(Code SAROA-FR-E-L-C) 1
A. E. Magistro
(Code SARPA-ND-D-B) 1
U. S. Army
Dover, NJ 07801

Harry Diamond Laboratory
Attn: J. T. Nelson
(Code DELHD-DE-OP) 1
Department of Army Material
Chief, Power Supply Branch
2800 Powder Mill Road
Adelphi, MD 20783

Scientific Advisor
Attn: Code AX 1
Commandant of the Marine Corps
Washington, DC 20380

Air Force of Scientific Research
Attn: R. A. Osteryoung 1
Directorate of Chemical Science
1400 Wilson Boulevard
Arlington, VA 22209

Frank J. Seiler Research
Laboratory, AFSC
USAF Academy, CO 80840 1

Dr. R. Burns
University of Illinois at Chicago
Department of Chemistry 1
Chicago, IL 60680

Boeing Aerospace Co.
Attn: S. Gross 1
C. Johnson 1
P.O. Box 3999
Seattle, WA 98124

Electrochemical Corporation
Attn: M. Eisenberg 1
2485 Charleston Road
Mt. View, CA 94040

Naval Coastal Systems Center
Attn: Library 1
Panama City, FL 32407

Naval Underwater Systems Center
Attn: J. Moden (Code SB332) 1
Newport, RI 02840

David W. Taylor Naval Ship
R & D Center
Annapolis Laboratory 1
Annapolis, MD 21402

Department National Defense
Attn: Library 1
Defense Research Establishment
Ottowa
Ottowa, Ontario K1A0Z4

NASA Johnson Space Center
Attn: Bob Bragg/EPS 1
Houston, TX 77058

Cordis Corporation
Attn: W. K. Jones 1
P.O. Box 525700
Miami, FL 33152

Tadiran
Attn: M. Babai 1
P.O. Box 75
Rehovot, Israel

Tel-Aviv University
Attn: E. Peled 1
Department of Chemistry
Tel Aviv, Israel 69978